ANL-FRA-163

ANL-FRA-163

ENGINEERING PHYSICS DIVISION

ENGINEERING PHYSICS DIVISION
ENGINEERING PHYSICS DIVISION
ENGINEERING PHYSICS DIVISION
ENGINEERING PHYSICS DIVISION
ENGINEERING PHYSICS DIVISION
ENGINEERING PHYSICS DIVISION
ENGINEERING PHYSICS DIVISION
ENGINEERING PHYSICS DIVISION
ENGINEERING PHYSICS DIVISION
ENGINEERING PHYSICS DIVISION
ENGINEERING PHYSICS DIVISION
ENGINEERING PHYSICS DIVISION
ENGINEERING PHYSICS DIVISION
ENGINEERING PHYSICS DIVISION
ENGINEERING PHYSICS DIVISION
ENGINEERING PHYSICS DIVISION
ENGINEERING PHYSICS DIVISION
ENGINEERING PHYSICS DIVISION
ENGINEERING PHYSICS DIVISION
ENGINEERING PHYSICS DIVISION
ENGINEERING PHYSICS DIVISION
ENGINEERING PHYSICS DIVISION

THE NEUTRONIC AND FUEL CYCLE PERFORMANCE OF INTERCHANGEABLE 3500 MWth METAL AND OXIDE FUELED LMRs

by

E. K. Fujita and D. C. Wade

BASE TECHNOLOGY

Argonne National Laboratory, Argonne, Illinois 60439
Operated by The University of Chicago
for the United States Department of Energy
Under Contract W-31-109-Eng-38

Argonne National Laboratory, with facilities in the states of Illinois and Idaho, is owned by the United States government, and operated by The University of Chicago under the provisions of a contract with the Department of Energy.

ANL-FRA-163

ARGONNE NATIONAL LABORATORY
9700 South Cass Avenue
Argonne, IL 60439-4801

THE NEUTRONIC AND FUEL CYCLE PERFORMANCE OF INTERCHANGEABLE 3500 MWth METAL AND OXIDE FUELED LMRs*

by

E. K. Fujita and D. C. Wade

Engineering Physics Division

MARCH 1989

*Work supported by the U.S. Department of Energy, Nuclear Energy Programs, under Contract No. W-31-109-ENG-38.

TABLE OF CONTENTS

LIST OF FIGURES

LIST OF TABLES

THE NEUTRONIC AND FUEL CYCLE PERFORMANCE OF INTERCHANGEABLE 3500 MWth METAL AND OXIDE FUELED LMRs

by

E. K. Fujita and D. C. Wade

ABSTRACT

This study summarizes the neutronic and fuel cycle analysis performed at Argonne National Laboratory for an oxide and a metal fueled 3500 MWth LMR. The oxide and metal core designs were developed to meet reactor performance specifications that are constrained by requirements for core loading interchangeability and for a small burnup reactivity swing. Differences in the computed performance parameters of the oxide and metal cores, arising from basic differences in their neutronic characteristics, were identified and discussed. It is shown that metal and oxide cores designed to the same ground rules exhibit many similar performance characteristics; however, they differ substantially in reactivity coefficients, control strategies, and fuel cycle options.

I. INTRODUCTION

Within the U.S. the emphasis for the deployment of LMR's have shifted from maximizing breeding and minimizing doubling time to enhancing safety, improving public acceptance, and minimizing capital costs. This changed emphasis in goals has motivated some new approaches to LMR core design and fuel management. In the U.S., recent core design efforts[1,2,3] have shifted from 1000 MWe and greater reactor sizes to much smaller outputs of 100 to 500 MWe. The U.S. core design activities have placed emphasis on the enhancement of the inherent reactivity feedbacks, larger thermal inertial attendant pool design, and the use of passive decay heat removal systems. In addition, the interest in metallic fuel has been renewed as a result of advances in metal fuel design[4] and the safety tests[5] conducted at EBR-II.

The focus of this study is to assess the neutronic and fuel cycle performance differences between metal and oxide fueled LMR's at a 3500 MWth rating. Traditionally the optimum reactor size was expected to be in the 1000 to 1350 MWe size range (2700 to 3500 MWth). Therefore, the current study characterizes the performance parameters of two representative 3500 MWth size cores. Detailed neutronic performance and safety characteristics are calculated and analyzed. Control system requirements are evaluated and compared against the available control rod worths. Differences in the computed performance parameters of metal and oxide cores which arise from basic differences in their neutronic characteristics will be identified and discussed.

II. CORE DESIGN DESCRIPTION

II.1 Ground Rules

The metal and oxide reactor core designs were developed based on the general reactor specifications summarized in Table I and the constraints of Table II. In addition, it was taken as a requirement to develop metal and oxide cores which are interchangeable in the following sense:

- same assembly pitch,
- same control rod locations and number of rods,

- same overall assembly length, and

- same (except for minor adjustments) radially heterogeneous core layout.

Detailed descriptions of the resulting core designs and their performance characteristics are given in the following sections.

II.2 Assembly Designs

The assembly and pin design parameters for the various assembly types are shown in Table III. The metal fuel assembly design is based on the designs used for the U.S. modular systems. It uses the ferritic HT-9 cladding and duct material, a 0.285 inch (7.239 mm) pin diameter with 0.75% smear density, and 271 pins per assembly. The large pin size is chosen to increase fuel volume fraction and core internal conversion ratio. The conservative clad thickness 0.022 in. (0.559 mm) and plenum to fuel length ratio of ~ 1.5 are consistent with the U.S. modular designs where a high temperature heat soak must be accommodated in the event of a passive decay heat removal transient.

The metal driver assembly is fluence limited at $35 \cdot 10^{22}$ fast neutron nvt. The 0.150 in. (3.81 mm) duct wall thickness and 0.200 in. (5.08 mm) inter-assembly gap was selected to accommodate the metal core conditions. The oxide assembly is geometrically identical to the metal assembly in the planar dimensions, and as a result is a little over designed in view of a lower fast neutron peak discharge fluence which results from the lower power density and the softer neutron spectrum in the oxide assembly.

The oxide pin contains 40 in. (1016 mm) of fuel and 14 in. (355.6 mm) upper and lower axial blankets of depleted UO_2 while the metal pin contains 36 in. (914.4 mm) of fuel and has no upper or lower axial blankets. The He-bonded oxide pin uses both upper and lower fission gas plena while the sodium-bonded metal pin has an upper plenum only. While the overall assembly length is taken to be identical for metal and oxide as a constraint, the differences in core fueled height, axial blanket thickness, and plenum location place the two core centerlines at different elevations.

The internal and radial blanket assemblies have an external envelope identical to that of the driver assembly. However, there are 169 pins in the blanket assemblies; each pin has a 0.392 in. (9.96 mm) outer diameter. The oxide blanket assemblies contain a

stack of UO_2 pellets 68 in. (1727.2 mm) high; the metal blankets are 36 in. (914.4 mm) high and of 85% smear density U10Zr alloy.

The removable radial shield assemblies are of two types. The first row of the radial shield consists of all steel assemblies, while the outer two rows of assemblies contain B_4C in pin form. The calculations used the ferritic steel, HT-9, for the inner rows as a preliminary choice; the use of nickel-containing steel to close the iron window will be examined, but has no major bearing on this calculational exchange.

II.3 Core Layouts

The active zone of the reactor is comprised of a radially heterogeneous arrangement of driver and internal blanket assemblies with one row of radial blanket and three rows of removable shield as shown in Figures 1 and 2 for the metal and oxide cross respectively. The components of the metal and oxide assembly lengths are summarized in Figure 3. The main motivations for using a radially heterogeneous arrangement rather than the homogeneous layout are:

- to obtain a less positive sodium density coefficient of reactivity,
- a higher internal conversion ratio for the given driver pin size, and
- a higher driver enrichment -- allowing for a lower fluence to burnup ratio in the fluence-limited metal driver assemblies.

The numbers of assemblies of various kinds are tabulated in Table IV.

The oxide core layout was optimized first. The optimization goals were:

- to obtain a low peaking factor
- which changes very little with burnup, and
- which peaks in the mid or outer core (where the primary control rods are)

and

- which keeps the peak linear heat rating (with discrete fuel management effects accounted for) below 13.5 kW/ft (285.8 kW/m) within the core height of 40 inches (1016 mm).

In addition, the optimization provided for 36 control rod positions which:

- are separated by no less than two assembly pitches so as to provide adequate space on the vessel head for rod drives, and

- have no more than two of the six assembly faces adjacent to blankets.

The metal core layout optimization, which was done second, required only that:

- six drivers in row 4 were replaced by internal blankets, while

- all else remains the same in the two layouts (with a decrease of core height to 36 inches (914.4 mm) and removal of axial blankets).

This fine adjustment relative to the oxide layout provided a better balance between peaking and burnup control swing for the metal neutronics.

It is noted that the burnup control swing calculation for this exercise represents only net fissile production vis-a-vis net absorber production and does not account for reactivity loss due to irradiation induced axial fuel growth in either metal or oxide fuel. While the axial growth effect cannot be ignored in detailed design for the metal cores, it is known that fine adjustments in the internal blanket smear density are capable of nullifying the reactivity loss of fuel axial growth with the reactivity gain from enhanced core internal conversion ratio. And as a result, a nominally zero burnup control swing can be designed. In that case the size of the TOP initiator will be dominated currently by the uncertainties in computing hot criticality and burnup swing, and will be dominated ultimately by the variability associated with manufacturing tolerances on fuel and structural components plus the variability in lockup properties of the core restraint system. Thus, for the purposes of this calculated inter-comparison, it is judged to be acceptable to neglect axial fuel growth.

II.4 Control Rod Banks

The layouts provide for 36 control rods whose locations are the same for the metal and oxide cores. These are divided into two independent systems of rods as shown in Table V. The primary control rod system serves both a safety and an operational function. This system has sufficient worth at any time in the reactor cycle to shut the reactor down from any operating condition, and to maintain subcriticality over the full range of temperatures expected during shutdown. Additionally, the primary control rod system meets fuel burnup and power control requirements for each cycle as well as compensating for criticality and refueling uncertainties.

The secondary control rod system has sufficient worth at all times in the reactor cycle to shut the reactor down from any operating condition to the hot-standby condition.

Both primary and secondary control rod systems are capable of performing their specified functions independently, and even with the failure of any single active component (i.e., a stuck rod). The required degree of subcriticality is taken to be 1$, consistent with the U.S. modular designs.

II.5 Fuel Management

The cores are designed for three year fuel residence time with one year refueling interval at 80% capacity factor. Under these conditions, relative to the constraints of Table II:

- the metal core is fluence limited*

  $31 \cdot 10^{22}$ peak fast nvt at 114.3 MWd/kg peak burnup

---

*Each core could perhaps accommodate a slight increase in driver residence time or in capacity factor or a reduction in core height. However, we instead retained those margins to accommodate the slight increases in local power density and flux which will result when discrete fuel management calculations are done explicitly.

while

- the oxide core is burnup limited*

  $23 \cdot 10^{22}$ peak fast nvt at 133.7 MWd/kg peak burnup.

The internal blankets remain in-core 3 years while the radial blankets remain in-core 6 years.

The isotopic composition of the plutonium comprising the fresh fuel feed was taken to be that isotopic distribution which is established in the fissile-self-sufficient closed metal fuel cycle in the equilibrium mode for the U.S. innovative reactor designs. This composition is shown in columns one and three of Table VI. The second and fourth columns of the table show that this composition closely approximates the closed cycle equilibrium composition which would be established in these larger cores as well. The last column of the table shows a typical LWR discharge composition for comparison.

While a discrete fuel management scheme has been developed for this layout, the purposes of this exchange can be met at lower computational cost by the "equilibrium cycle" approximation discussed in the next section.

III. CORE PERFORMANCE CHARACTERISTICS

III.1 Methodology

A neutronics analysis was carried out for the metal and mixed oxide heterogeneous core designs described above. The major objective of these analyses was to establish the relevant performance parameters needed for performing safety evaluations.

The basic cross section data used for the neutronics analyses were ENDF/B-V.2. These data were processed through the MC^2-2/SDX code system[6,7] to generate separate oxide and metal fuel broad-group libraries which explicitly take account of resonance and spatial self-shielding effects. Nine group cross section sets were generated for general use (in the depletion and rod worth calculations) and twenty-one group sets were generated for the reactivity coefficient calculations.

Burnup calculations were carried out in three-dimensional hexagonal-z geometry using the REBUS-3 code[8] and a nodal diffusion theory neutronics methodology[9] based on the equilibrium cycle approximation. In this computational approximation the driver and blanket compositions are each spatially smeared at BOEC -- assuming a scatter reload of 1/3 of the assemblies (1/6 of the radial blanket assemblies) -- after the enrichment of the fresh fueled assemblies has been adjusted so as to yield a just-critical reactor at EOEC. As a result of the spatial smearing of the fresh and the partially burned compositions for computational ease, the local power peaking which occurs at BOEC when a fresh assembly is loaded into a position next to partially burned assemblies is not modeled explicitly in the hex-Z flux solution used for depletion nor in the edited peak power density. Moreover, the depletions are performed with all rods withdrawn to the top of the fuel. The core performance evaluations of succeeding sections are based on this equilibrium cycle neutronics approximation which, in separate studies, has been shown to be quite accurate for global performance parameters. On the other hand, the thermal/hydraulics evaluations and the orificing flow allocations do take account of the assembly-wise local power peaking which arises upon introduction of a fresh driver into a sea of partially burned neighbors by using an approximation based on multiplying the assembly average flux from the equilibrium cycle calculation by the ratio of fresh to BOEC-assembly-smeared macroscopic fission cross section.

The sodium void, sodium density, Doppler coefficient, fuel and structure worths and axial and radial expansion coefficients of reactivity were determined in three-dimensional hex-Z geometry for end-of-equilibrium cycle (EOEC) conditions. Flux and adjoint distributions were calculated in 21 energy groups using the DIF3D code[10], and these data were input to VARI3D to generate the appropriate reactivity worth coefficients.

Control rod worths were calculated in hex-Z geometry. However, the stuck rod worths were calculated in 2D hex geometry using the full planar core layout. Azimuthal tilts which result from asymmetric rod insertion or withdrawal patterns are thereby scoped in that azimuthal tilts are smaller when the rods are only partially inserted.

III.2 Equilibrium Cycle Performance

A) Mass Flows

The equilibrium cycle mass flows are shown in detail in Tables VII and VIII for the metal and oxide cores, respectively. Table IX summarizes several of the salient differences between the oxide and metal cores.

The oxide heavy metal loading and heavy metal mass flows are substantially larger than those of the metal core mostly because of the presence of the 14 inch axial blankets and the correspondingly taller blanket assemblies, but also because of the taller core. In particular, the oxide reactor (i.e. core plus blankets) volume is some 70 percent larger than the corresponding metal reactor volume, and this more than compensates for the lower heavy metal smeared density of the oxide vs. the metal fuel form. While the 40 inch core height is required based on pin peak linear heat rating and the goal of interchangeability in oxide/metal layout, and cannot be reduced, one could, if desired, reduce the oxide axial blanket thickness, with corresponding reductions in internal and radial blanket lengths, as a way to reduce the heavy metal reprocessing/refabrication mass throughputs -- since the oxide breeding ratio is ten points higher than that of the metal core. This would have only small effects on safety coefficients, linear heat rate and burnup control swing which are the focus of this calculational exchange. Thus, we elected instead to retain the traditional oxide goal of a ~1.2 breeding ratio and separately maintain the traditional IFR goal of a net fissile production which is only just sufficient to overcome estimated reprocessing/refabrication losses.

The oxide enrichment, initial fissile inventory, and fissile loading/year all exceed those of the metal core basically because of the softer neutron spectrum and the lower U^{235} loading to the internal blankets. The harder spectrum of the metal core both increases η and leads to more U^{238} fast fission effect thereby giving a higher worth pwer gram of fuel and requiring a lower enrichment for BOEC criticality. Tables X and XI show the neutron balances for the two cores. The higher η and fast effect plus the increased amount of U^{238} in the core increase the internal conversion ratio of the metal metal core relative to oxide so that a lower BOEC enrichment is required to assure EOEC criticality. In fact as shown in Table VII, the metal core gains ~ of reactivity per cycle vis-a-vis a ~$2 loss of reactivity per cycle for the oxide core.

---

*The TOP initiator is about the same for the two cores -- but occurs at different times in life.

B. Power Distributions

The power fractions for the different regions of the reactor at BOEC and EOEC are shown in Table XII. The driver plus internal blanket power fractions are 2 to 3% higher in the metal core than the oxide because of the absence of axial blankets.

In optimizing the layouts shown in Figs. 1 and 2, major emphasis was placed on lowering, positioning, and stabilizing the peak/average power density ratio -- the peaking factor. The Fig. 2 layout for the oxide core resulted from a substantial effort in this regard, and as shown in Table XIII produced a core whose power peaking factor was 1.44 at BOEC and 1.52 at EOEC -- within the equilibrium cycle modeling approximation**. Moreover, as shown in Table XIII, the peak occurs in the outer core at BOEC and shifts to the middle core by EOEC. This avoidance of inner core peaking enhances the worths of the primary control rods located in the outer core regions. Finally, the burnup control swing for this large-pin, optimized oxide core was only ~$2 loss in reactivity over one cycle.

When the metal core assemblies were used with the core layout optimized for oxide properties, Fig. 2, their different internal conversion ratio performance caused the power peaking factors (1.51 at BOEC and 1.63 at EOEC) to shift inward (middle core at BOEC and inner core at EOEC) as shown in the last two columns of Table XIII. Moreover, the burnup control swing was a ≈$3 increase in reactivity over one cycle. However, the stability of power distribution which had been achieved in the oxide layout allowed us to fine tune for the metal neutronics performance with only a minor change; i.e. to replace 6 drivers in row 4 with internal blankets. This change restored the radial power profile and its balance -- shifting the peaking factor outward 1.42 (outer core) at BOEC and 1.49 (middle core) at EOEC. Moreover, the outward shift of power lowered the gain in reactivity over one cycle to about $2. Table XIII summarizes these results.

Table XIV summarizes the peak linear heat ratings for the metal and oxide core layouts of Figs. 1 and 2 respectively. The lower part of the table includes the effect of fresh assembly power peaking in the approximate way described previously -- which is known to be accurate with respect to more detailed analyses of discrete fuel

---

**Fresh fuel assembly effects would raise the BOEC value by about 15%.

management. The oxide fuel pins remain below the rule-of-thumb limit of 13.5 kW/ft set by fuel centerline temperature considerations, with the EOEC peak in the IB only slightly exceeding the BOEC peak in the driver. With the shorter core length, the metal fuel peak linear heat rating occurring in the driver pins is 13.9 kW/ft and remains below the rule-of-thumb 15 kW/ft limit set jointly by fuel centerline and fuel/clad interface temperature considerations. Alternately, because of the larger shift of power into the internal blankets which results from the metal core's higher U^{238} concentration in blanket pins, the EOEC blanket pin peak linear heat rating is 15.6 kW/ft. The increase in fuel alloy solidus temperature with decrease in plutonium content allows for a higher heat rating on blanket metal pins than in driver pins, so the 15.6 kW/ft lies within design constraints.

C) Discharge Fluences and Burnup

Table XV summarizes the peak and average burnups by assembly type for the metal and oxide cores while Table XVI summarizes the peak discharge fast neutron fluence. The average discharge burnups of the drivers differ as a result of different heavy metal content in the drivers and different blanket power fractions.

The metal core drivers are fluence limited with peak discharge conditions of $31 \cdot 10^{22}$ fast nvt and only 114.3 MWd/kgHM. Alternately, for the oxide core, the fast neutron flux level is reduced relative to the metal core for two main reasons. First, the average power densities are lower because of the taller core and second, the oxide core neutron spectrum is softer with a higher fraction below 0.1 MeV because of the oxygen scattering*. The result is that the oxide core experiences driver peak discharge conditions of only $23 \cdot 10^{22}$ fast nvt for a burnup of 133.7 MWd/kgHM and thus is burnup limited.

While the metal core radial blanket peak discharge fluence at 6 years residence time is $38 \cdot 10^{22}$ fast nvt, this point wise maximum would in practice be eliminated by blanket assembly rotation part way through life and therefore is not viewed with concern.

---

*The higher enrichment and lower effective heavy metal density of the oxide fuel relative to the metal fuel tend to cancel such that the fissile atom densities of the two cores differ by less than ten percent; as a result enrichment differences are not the cause of the discharge fluence differences.

D) Control Rod Systems

Tables XVII and XVIII show the control requirements for the primary and secondary rod banks for the metal and oxide cores, respectively. In conformance with U.S. practice, the primary rod bank is used:

- to compensate fuel burnup control swing,
- to control power level,
- to trim small reactivity variations due to manufacturing tolerances, structural variations, etc., and
- to achieve reactivity scram.

The primary bank is required to be capable of taking the core to subcritical at reload temperature even with one stuck rod.

The secondary rod bank, which is positioned at its fully withdrawn position at normal operating conditions, is used:

- to provide a diverse, redundant scram capability,

and must be capable of taking the core to subcritical at hot standby temperature.

Here we define subcritical to imply greater or equal to 1$ in conformance with the U.S. modular design practice.

In Tables XVII and XVIII the "Hot-to-Cold" component compensates for the net reactivity insertion due to the Doppler effect, radial and axial contraction, and sodium density changes during reactor shutdown from the full-power operating temperature to the refueling or hot standby temperature. The reactivity effect of thermally induced core contraction is approximated based on coefficients of thermal expansion of the duct and pin clad structural material and on expansion reactivity loss coefficients which are computed by eigenvalue difference for uniform radial dilation of all material internal to the core/radial reflector interface and for uniform axial dilation over the core fuel height.

The "Maximum Reactivity Excess" component in Tables XVII and XVIII accounts for the burnup control swing plus uncertainties and represents the maximum possible reactivity excess at the BOEC, hot operating, all rods out condition. It is estimated using the formula:

$$\text{Max Reactivity Excess} = 1.15 * (\text{Burnup Control Swing}) + 0.2\%\ \Delta k$$

and, in these cores, is small because the burnup control swing is itself small*.

The low burnup control swing also leads to a low control requirement imposed on both control systems for the "Rod Runout Reactivity Fault". This Rod Runout Reactivity Fault is determined from the Maximum Reactivity Excess, including uncertainties, which must be suppressed by a primary control rod bank, taking into account a first-out rod interaction effect of 150%. Since this rod runout reactivity fault requirement is so small, an alternative, more demanding requirement is imposed to determine control system requirements. It is that both primary and secondary control systems must retain a suitable "Shutdown Margin". For the purposes of this study, a shutdown margin of 1$ was assumed. In computing the ability to meet this margin, the control requirement for cold criticality prediction uncertainty of 0.3% Δk which was used for Clinch River is adopted here. The control requirement for fissile refueling tolerance, 0.3% Δk, is based on a 0.5% uncertainty in batch fissile enrichments.

Based on the above considerations, the maximum reactivity control requirements, including uncertainties, for the primary and secondary control systems are 1.878 and 0.626% Δk, respectively for the metal core and 2.465 and 1.246 % Δk for the oxide core. The larger Doppler component in the hot-to-cold swing is the main reason for the larger requirements in the oxide core.

Tables XIX and XX show, for the metal and oxide cores respectively, that natural B_4C rods meet the control requirements with margin. In fact only a small increase in B^{10} enrichment would be required if it were desired to use a 1% Δk rather than 1$ shutdown requirement.

---

*Note that the formula uses the absolute value of the burnup swing, and for the metal core which gains reactivity with burnup, the Maximum Reactivity Excess occurs at EOEC.

Figures 4 and 5 display the primary control bank worths as a function of insertion depth for the metal and oxide cores, respectively.

E) Reactivity Coefficients

The prompt neutron lifetime and delayed neutron fraction were calculated using 21 group sodium-in real and adjoint fluxes from a 3D hex-Z finite difference model. The ENDF/B-V.2 delayed neutron data were used for all fissionable isotopes. The results are given in Table XXI.

Table XXII shows the global reactivity coefficients evaluated at EOEC for both the metal and oxide cores.

The sodium worth calculation was performed using first order perturbation theory in a 21 group hex-Z finite difference model. In particular the flooded real flux and adjoint flux were used with a perturbation defined by voiding the flowing sodium from the core and axial blankets. Both the number densities of sodium and the microscopic cross sections for all isotopes (reflecting the changes in spectrum and in self-shielding) were changed in defining the perturbation. The leakage term was treated rigorously. The sodium density coefficient of reactivity was computed in a way similar to the sodium void worth except that all isotopic microscopic cross sections retained their sodium-flooded values.

Two sets of Doppler reactivity calculations were performed; sodium-in and sodium-out. For the former calculation, flooded real and adjoint fluxes were generated in a 21 group hex-Z finite difference model, and for the latter the real and adjoint fluxes were calculated for sodium voided from the core and blankets. These calculations used the appropriate (Na-In, Na-Out) cross sections with all fuel isotopes at 1300°K for the oxide base case and 850°K for the metal base case. The Doppler reactivity for the fuel was calculated by perturbing the cross sections of the heavy metal to reflect a temperature of 2600°K for the oxide and 1700°K for the metal. Doppler reactivity for the structural material (fuel pin clad and duct wall) was calculated as well. Here the base case temperature of the structure was 750°K and the perturbed structure cross sections were at 1500°K for both metal and oxide.

Radial and axial expansion reactivity loss coefficients ($/cm) are computed, for example, by eigenvalue difference for uniform radial dilation of all material; then divided by the change in radius of the core/radial blanket interface or alternately, for uniform axial dilation over the model; then divided by the change in core fuel height. A 9 group hex-Z nodal model was used.

Control rod bank differential worths at their BOEC and EOEC full power operating positions are computed by eigenvalue difference in hex-Z model (9 group) using a special model with fine axial mesh near the rod tips. The purpose of these coefficients is for the accounting for control rod driveline expansion in ATWS accident analyses. Table XXIII shows the locations of the rod tips at BOEC and EOEC.

Examination of Table XXII shows that the harder spectrum of the metal core leads to a sodium void worth and sodium density coefficient which are about 33 percent more positive than those of the oxide. The fuel and the Doppler coefficients are somewhat less than half as negative for the same reason. Alternately, the radial and axial expansion coefficients, which are determined mostly by core size and H/D ratio, have similar values for the two cores.

Reactivity worth distributions have also been generated in the format required by the SAS codes[111] (which are used for evaluation of transient and safety performance). Figure 6 displays the SAS-Channel numbers to which the metal assemblies were assigned and Figure 7 displays the corresponding information for the oxide assemblies. Table XXIV shows the axial mesh intervals used for each channel and Figures 8-16 illustrate the computed worth profiles for the metal core at EOEC. Table XXV shows the axial mesh intervals used for each channel and Figures 17-25 illustrate the computed worth profiles for the oxide core at EOEC.

IV. CONCLUSIONS

In this study, we have identified and quantified those physics parameters which differentiate metal and oxide fuel types when the cores are designed to meet the constraints of interchangeability and small burnup reactivity swing. The study shows that although oxide and metal cores designed to the same ground rules may exhibit many similar performance characteristics, they differ substantially in reactivity coefficients, control strategies, and fuel cycle operations. The metal fueled core was shown to offer some important performance advantages over the oxide core because of its harder neutron spectrum, and resultant superior neutron economy and greater breeding potential. These advantages include smaller fissile and heavy metal loading and reduced control system requirements and control rod boron enrichment level.

However, the more important differences relate to differences in transient and safety performance which derive from differences in reactivity coefficients and thermal conductivity of the fuel forms; these differences are covered in a companion study[12].

V. ACKNOWLEDGMENTS

The authors would like to acknowledge S. F. Su for the layout selection trade studies and H. S. Khalil for his work on the effect of discrete fuel management on reactor performance parameters predicted by the equilibrium cycle analysis.

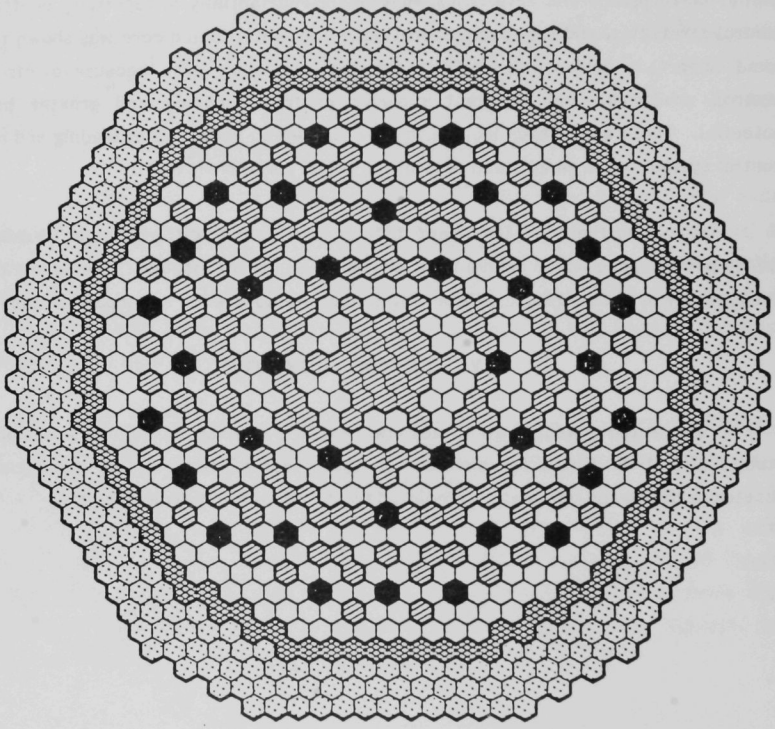

FIGURE 1. METAL CORE PLANAR LAYOUT

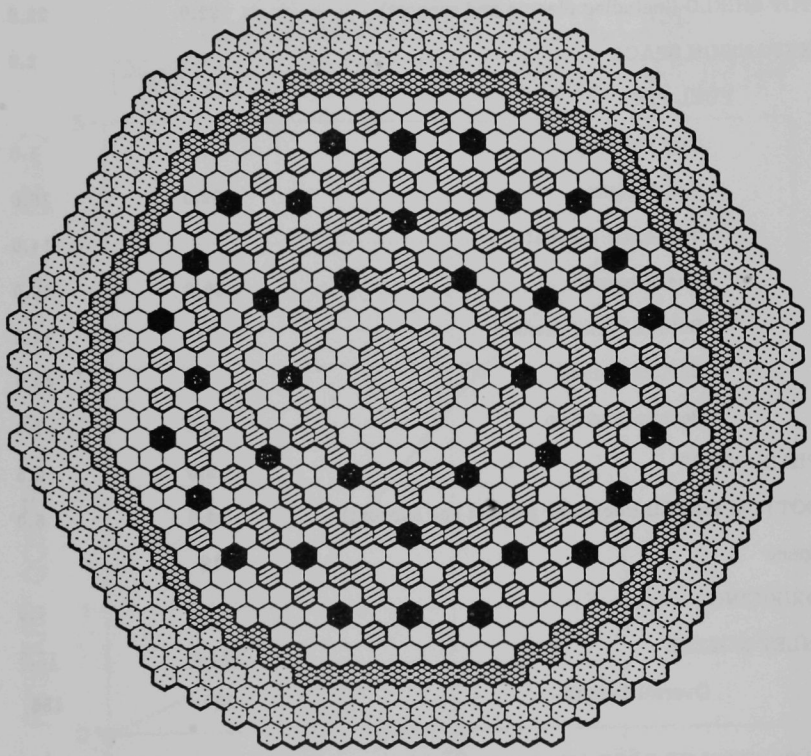

FIGURE 2. OXIDE CORE PLANAR LAYOUT

COMPONENTS OF ASSEMBLY LENGTH (in.)*

	METAL	OXIDE
TOP END FITTING 9.0	9.0	
TOP SHIELD (including plenum and support)	22.0	22.0
EXPANSION SPACE	2.0	2.0
FUEL PIN		
Top End Cap	1.0	1.0
Top Plenum	52.0	16.0
Top Axial Blanket	-	14.0
Fuel Region	36.0	40.0
Bottom Axial Blanket	-	14.0
Bottom Plenum	-	40.0
Bottom End Cap	1.0	1.0
PIN SUPPORT	2.5	2.5
BOTTOM SHIELD (including plenum and support)	24.0	6.0
Space	18	-
ORIFICING	4.0	4.0
INLET NOZZLE	13.5	13.5
Overall Length	185	185
ELEVATION OF CORE AXIAL MID-PLANE RELATIVE TO BOTTOM OF ASSEMBLY	81.0	101.0

*These length selections are based on prior experience and do not benefit from either explicit shielding calculations or explicit core restraint analyses or explicit pin analyses -- to determine plenum length. They should be viewed as quite preliminary.

FIGURE 3

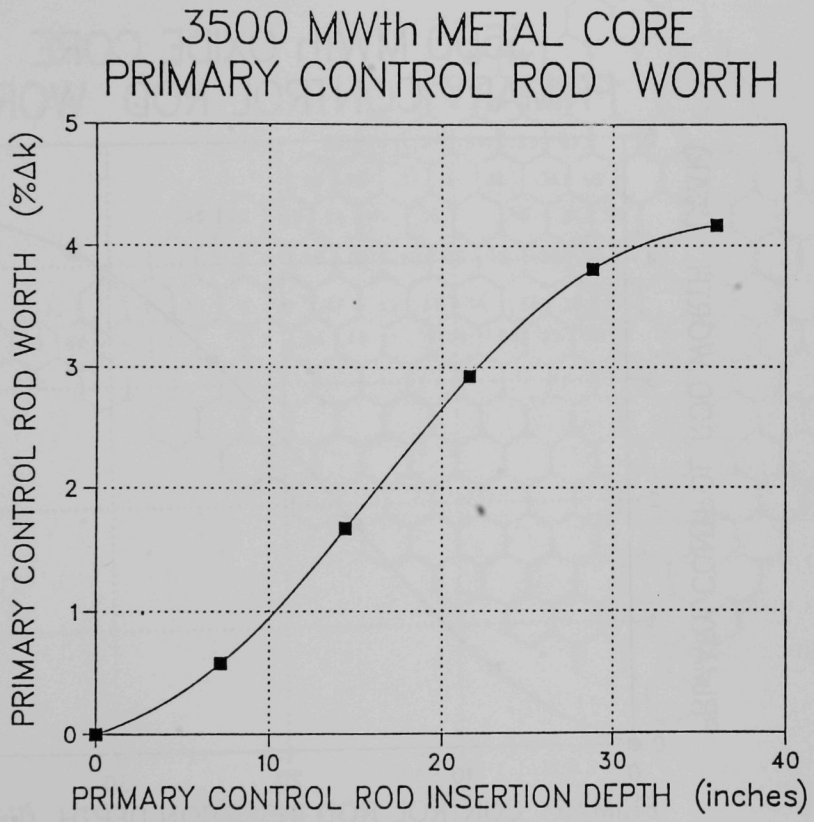

FIGURE 4. METAL CORE PRIMARY CONTROL WORTH vs. INSERTION DEPTH

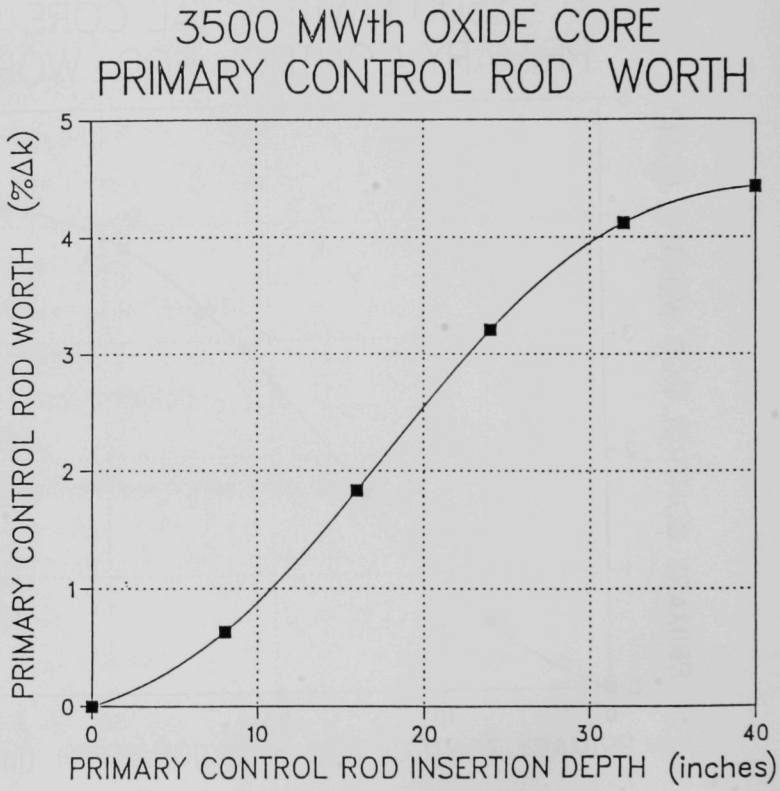

FIGURE 5. OXIDE CORE PRIMARY CONTROL WORTH vs. INSERTION DEPTH

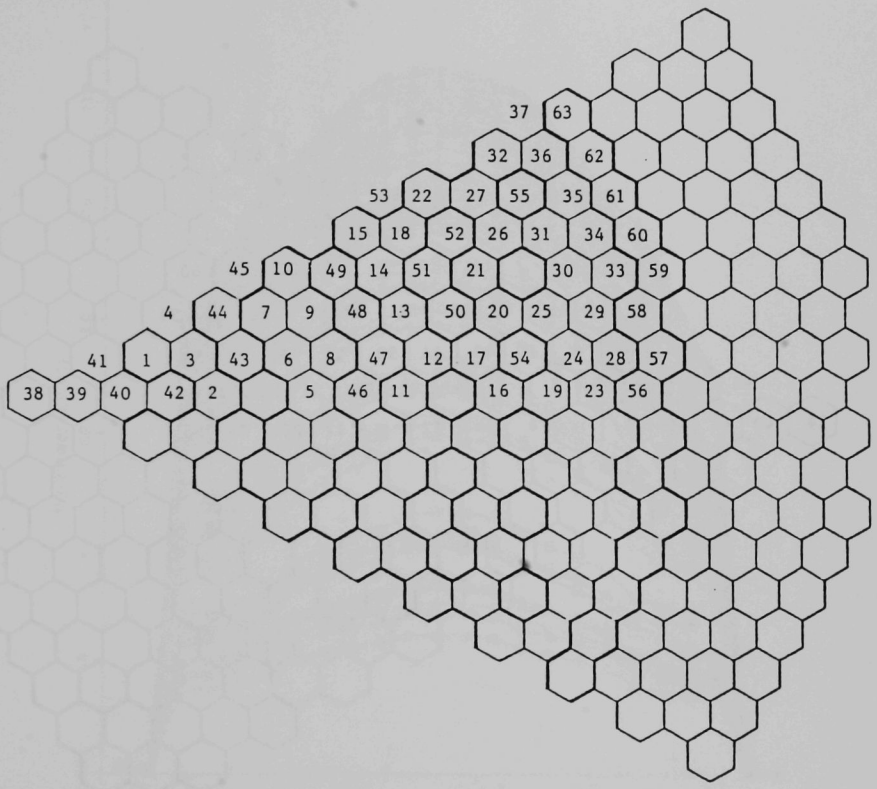

FIGURE 6. METAL CORE ASSEMBLY TO SAS-CHANNEL ASSIGNMENT

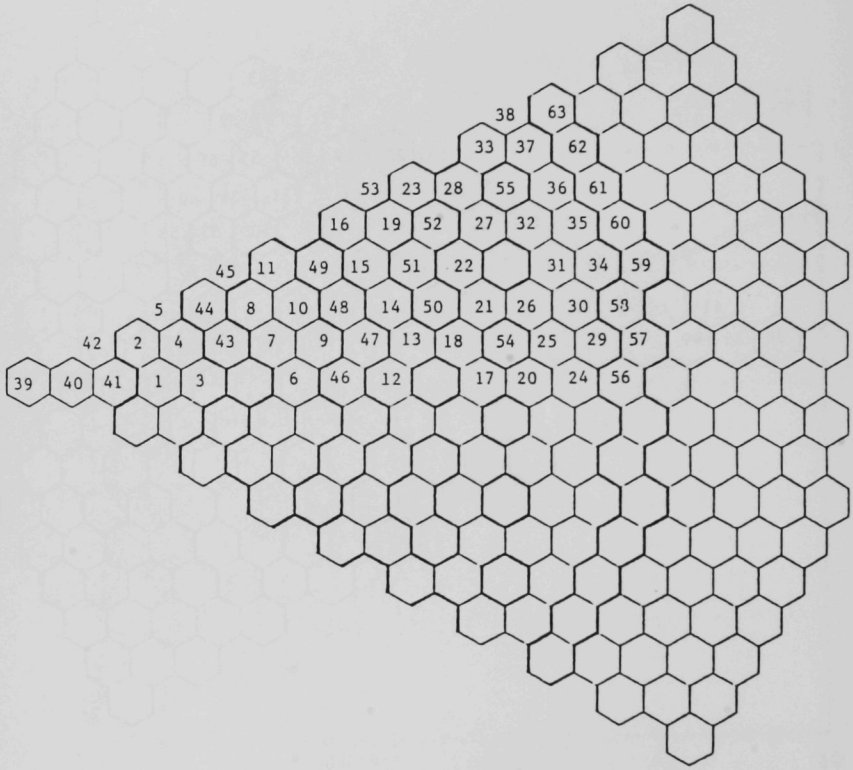

FIGURE 7. OXIDE CORE ASSEMBLY TO SAS-CHANNEL ASSIGNMENT

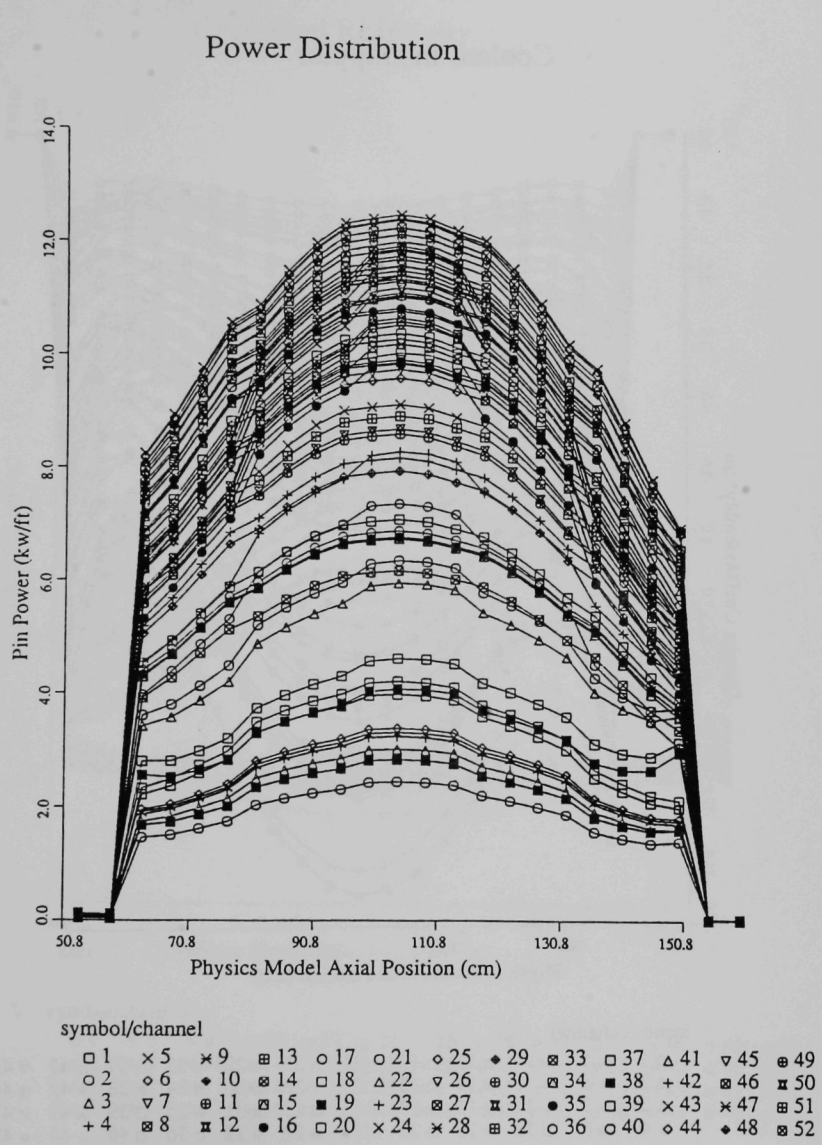

FIGURE 8. METAL CORE PIN POWER BY SAS-CHANNEL AT EOEC

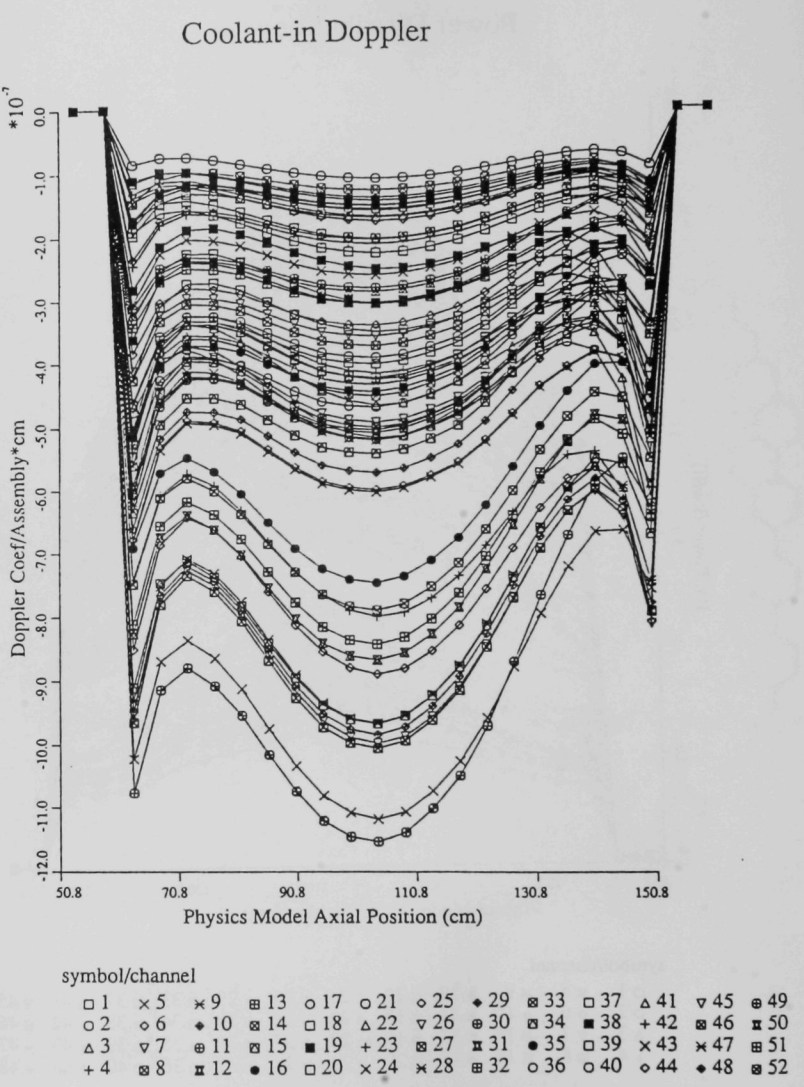

FIGURE 9. METAL CORE FLOODED DOPPLER WORTH AT EOEC

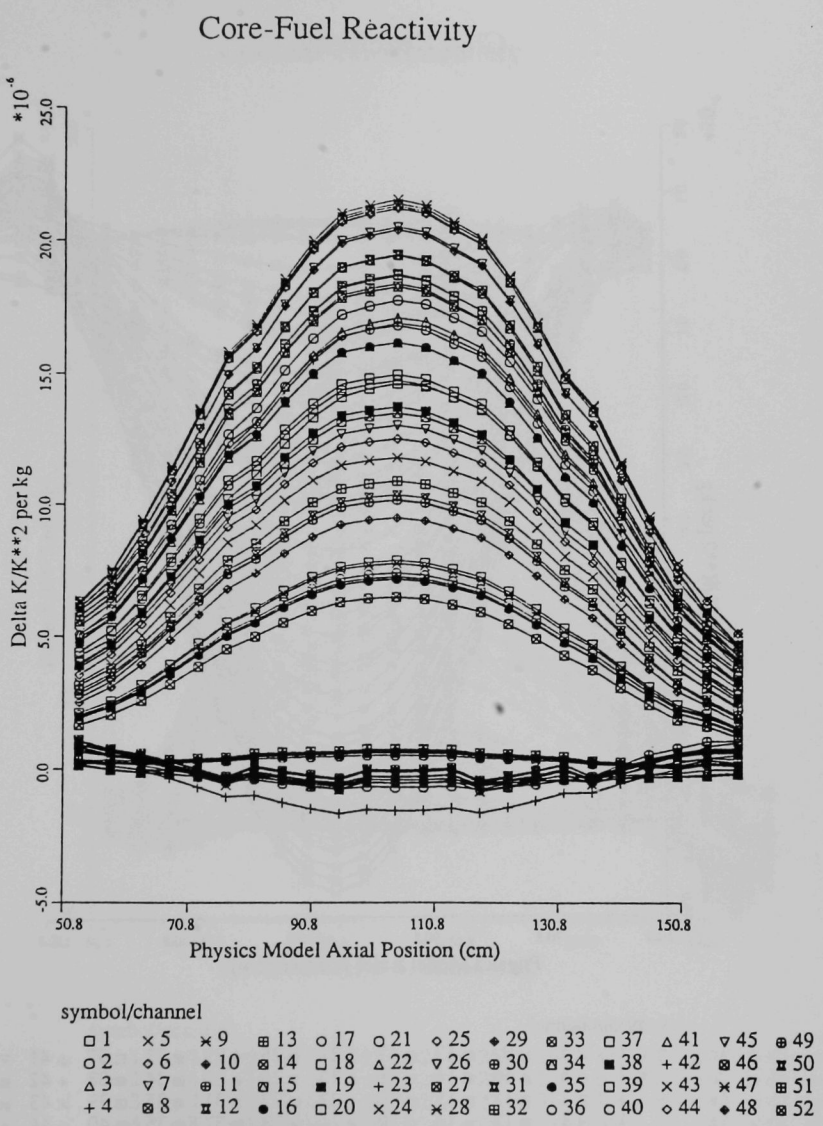

FIGURE 10. METAL CORE FLOODED FUEL WORTH AT EOEC

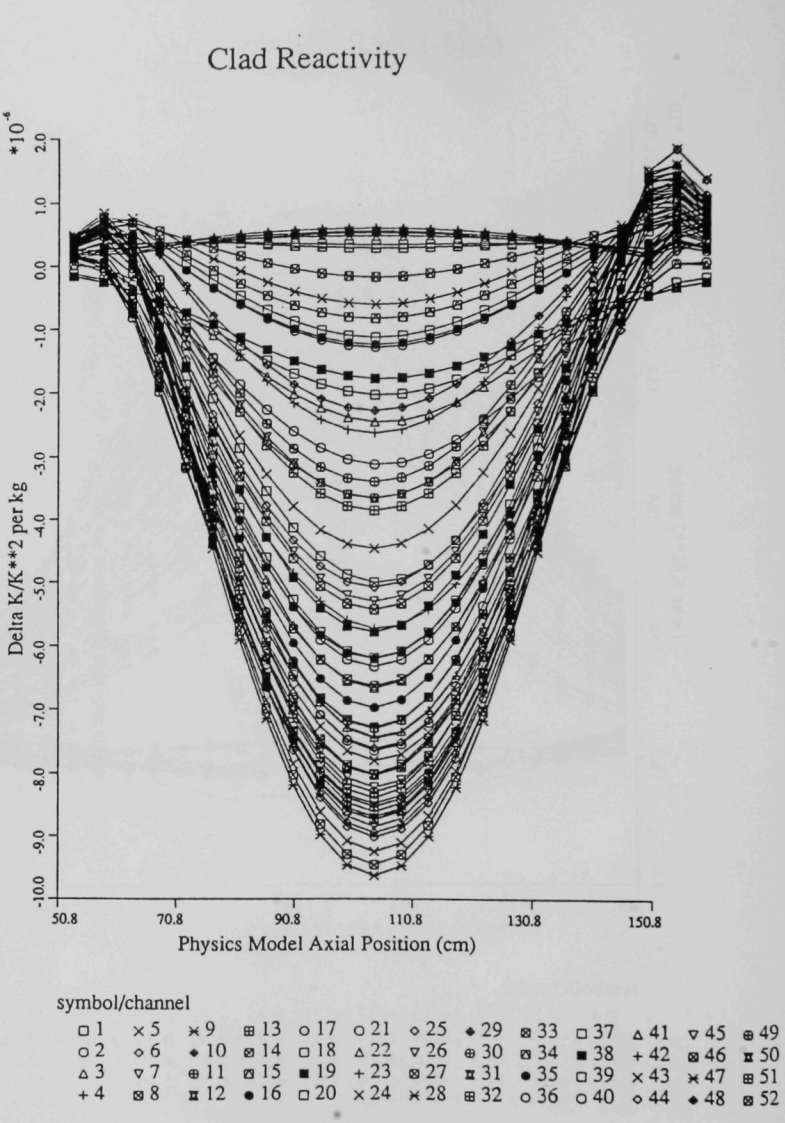

FIGURE 11. METAL CORE FLOODED CLAD WORTH AT EOEC

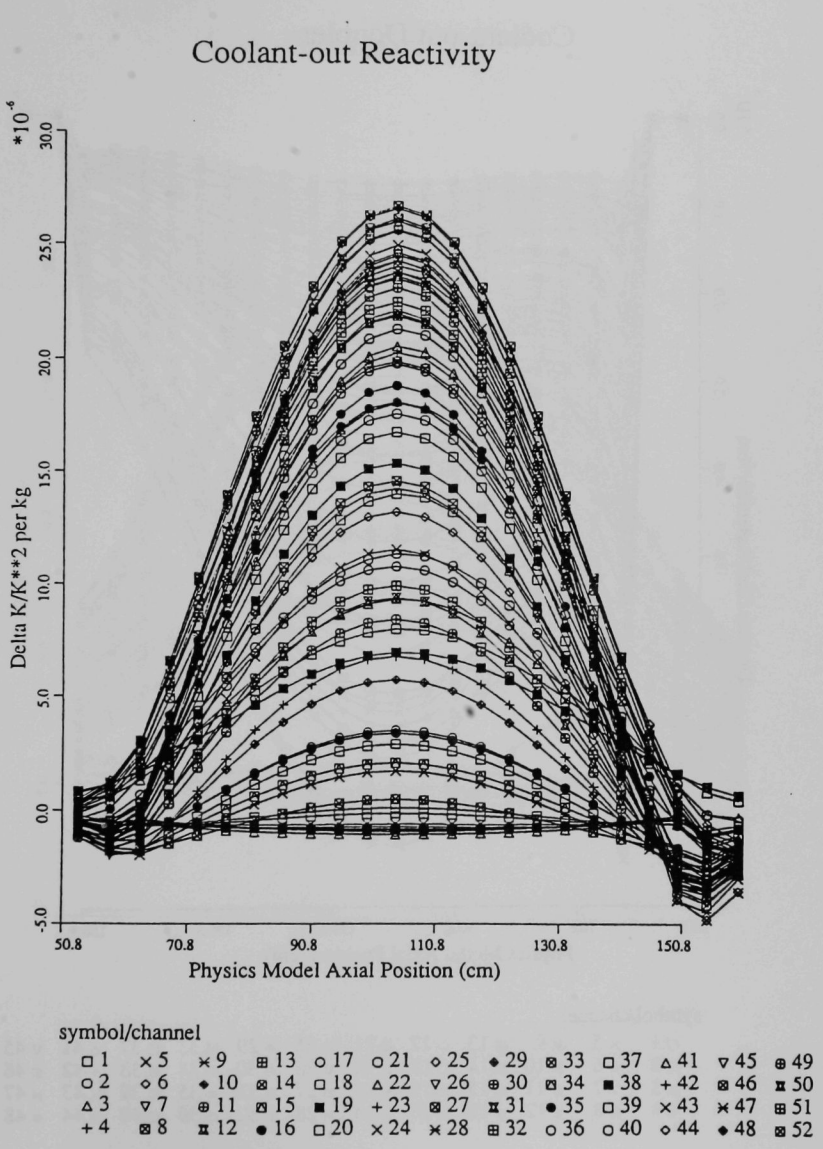

FIGURE 12. METAL CORE SODIUM DENSITY WORTH AT EOEC

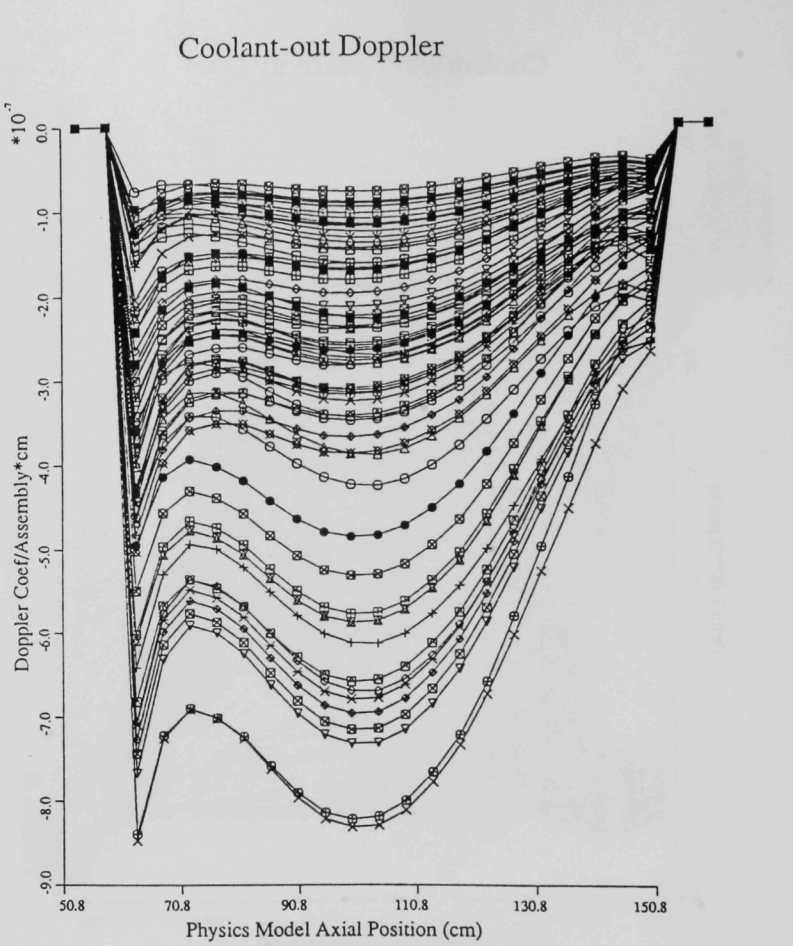

FIGURE 13. METAL CORE VOIDED DOPPLER WORTH AT EOEC

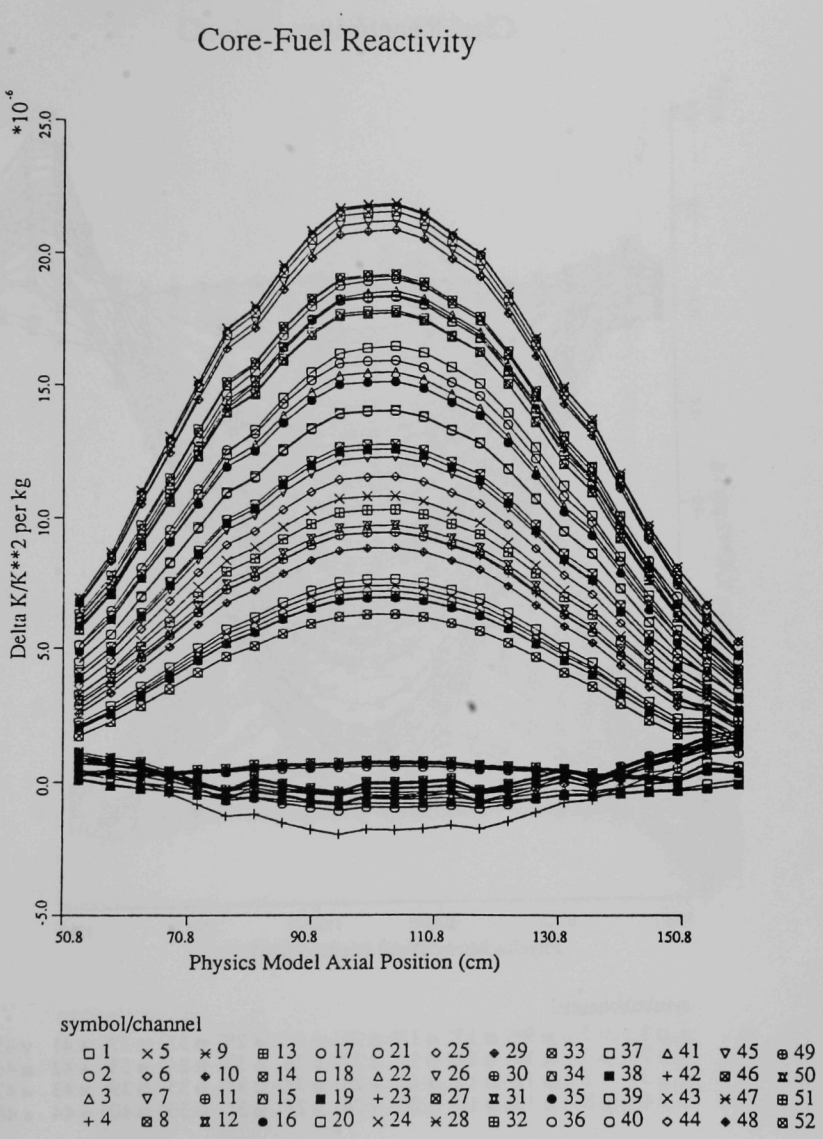

FIGURE 14. METAL CORE VOIDED FUEL WORTH AT EOEC

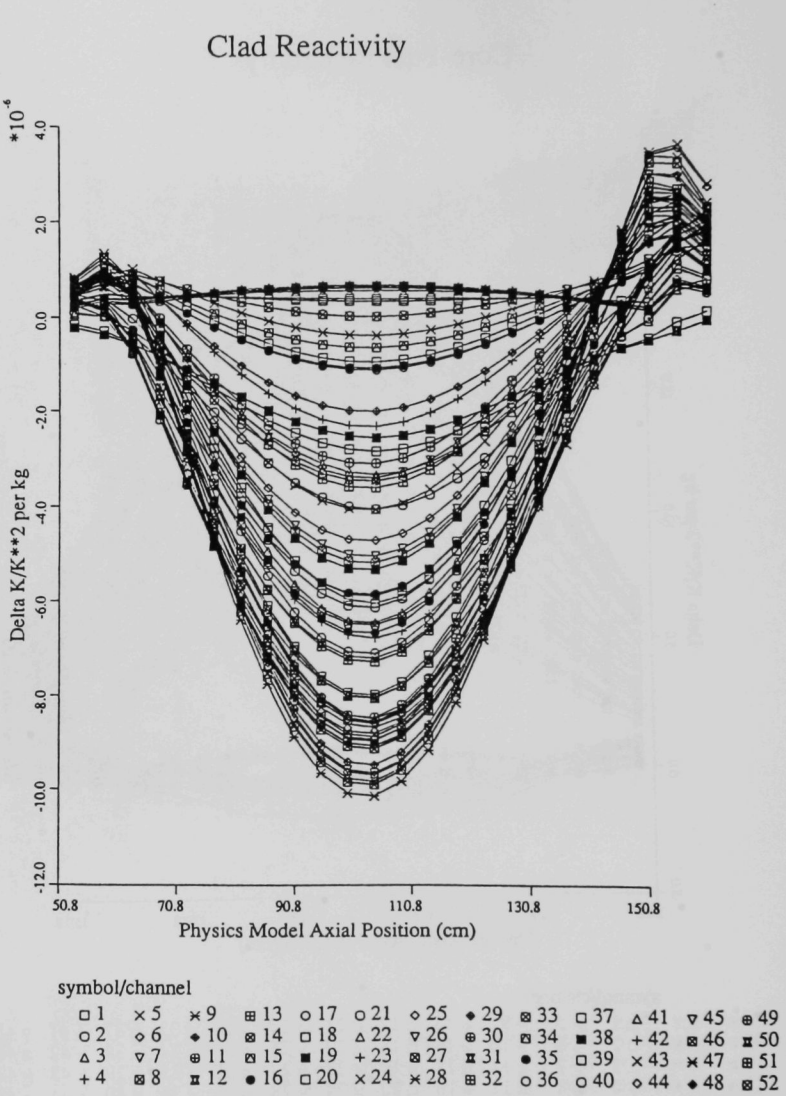

FIGURE 15. METAL CORE VOIDED CLAD WORTH AT EOEC

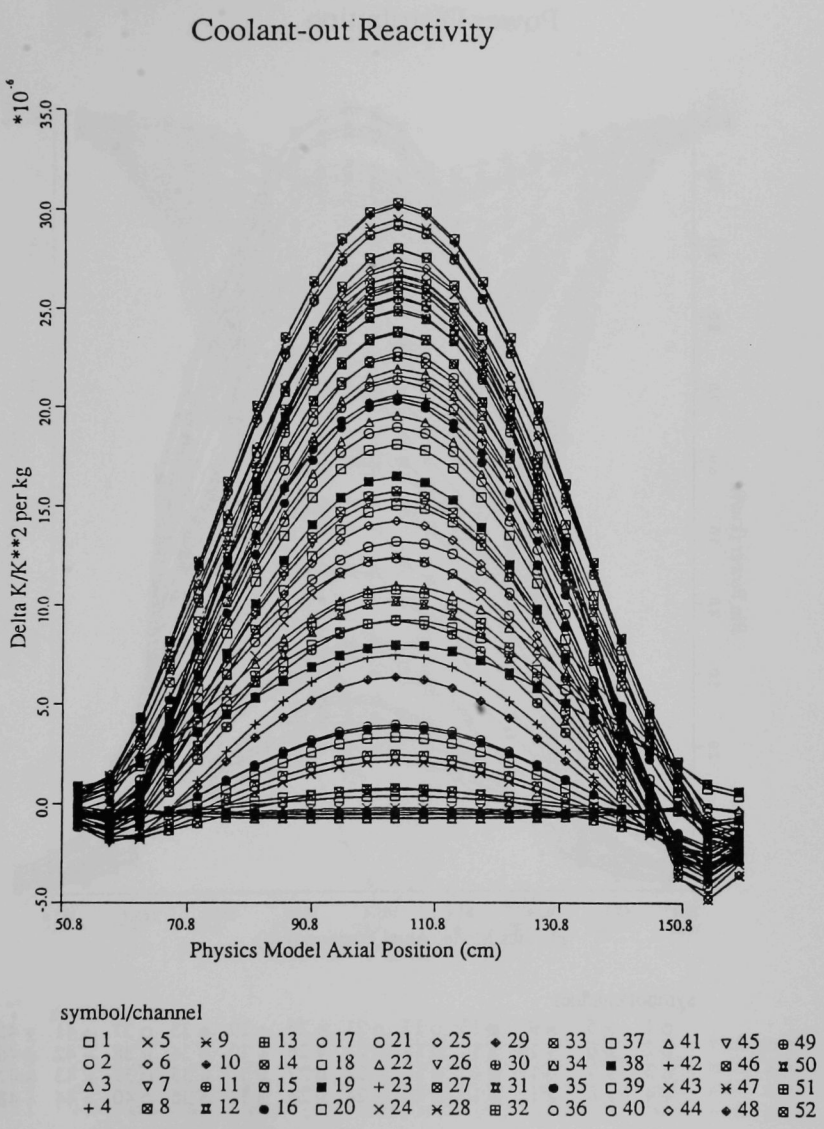

FIGURE 16. METAL CORE SODIUM VOID WORTH AT EOEC

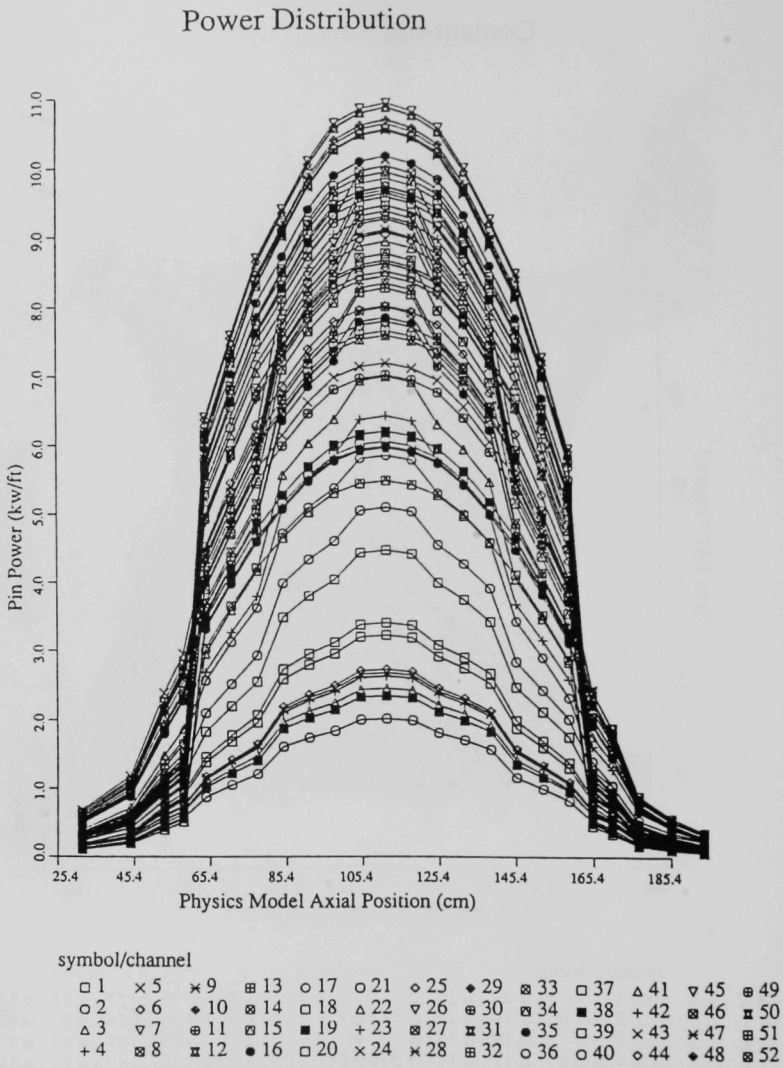

FIGURE 17. OXIDE CORE PIN POWER BY SAS-CHANNEL AT EOEC

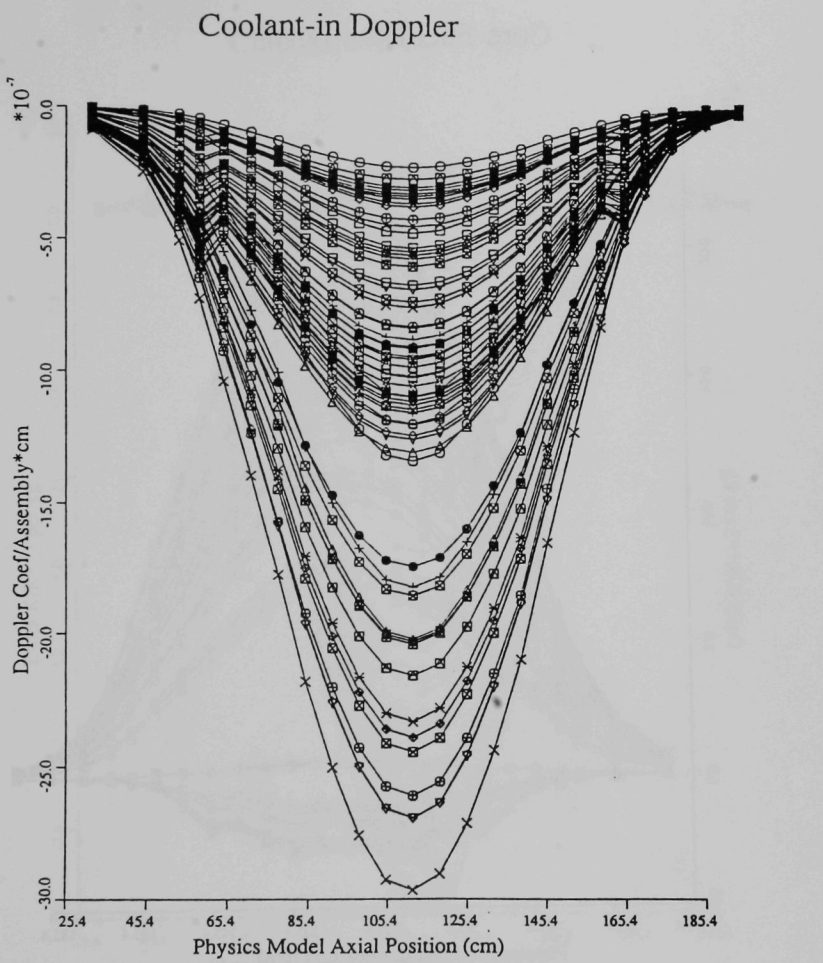

FIGURE 18. OXIDE CORE FLOODED DOPPLER WORTH AT EOEC

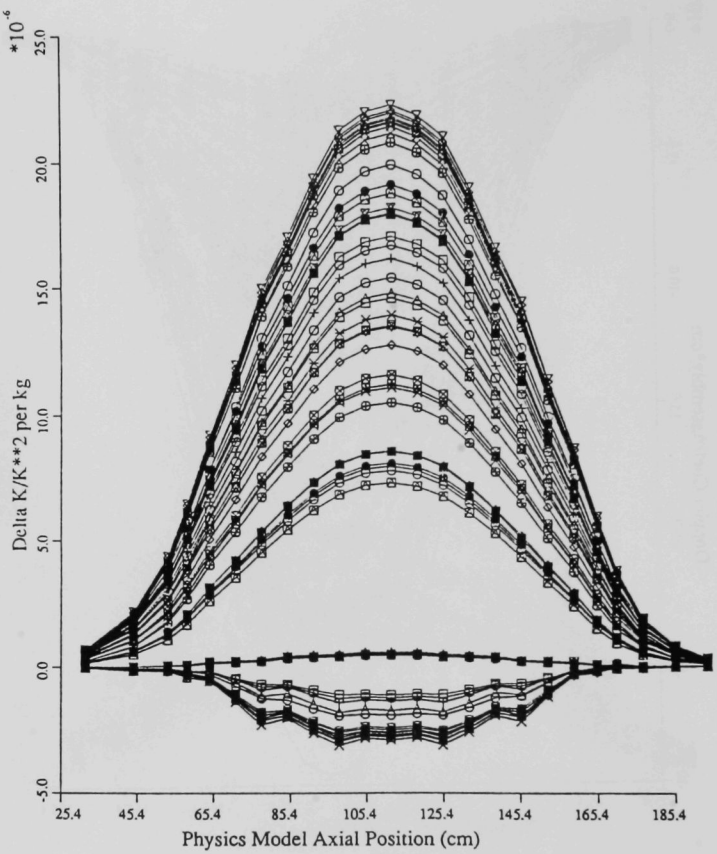

FIGURE 19. OXIDE CORE FLOODED FUEL WORTH AT EOEC

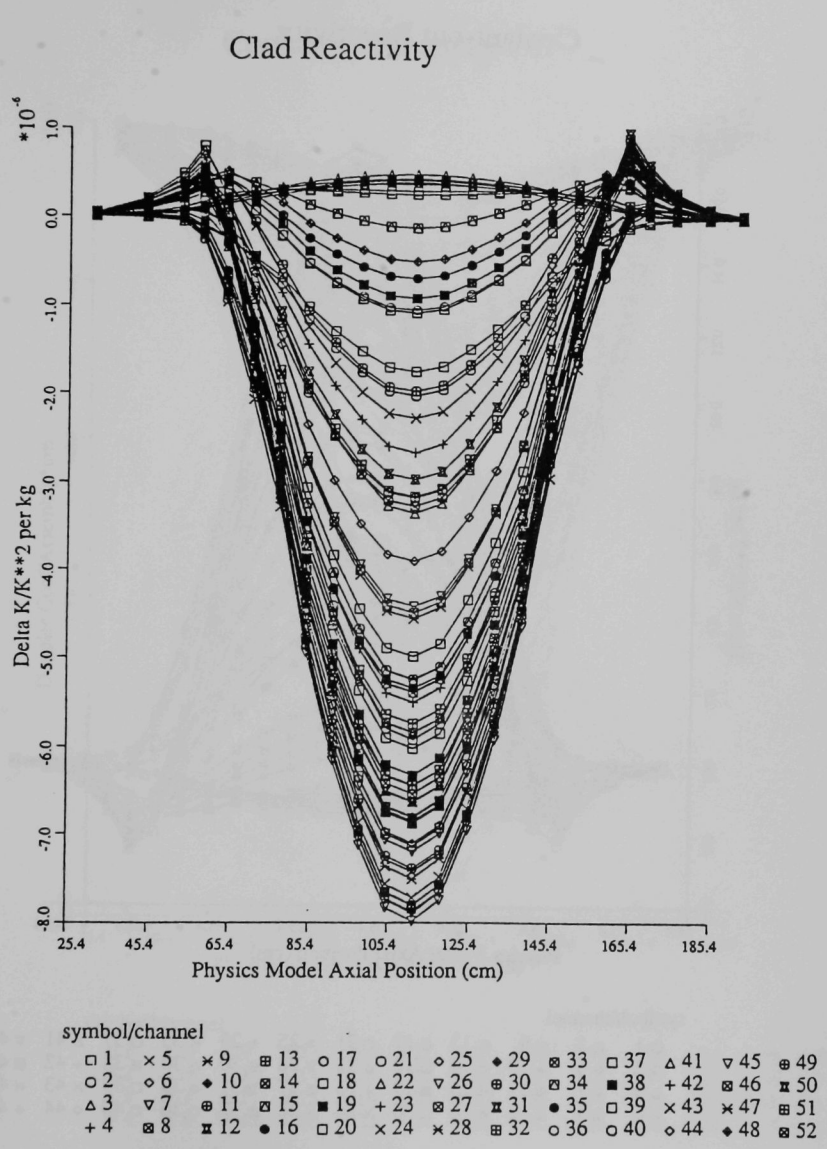

FIGURE 20. OXIDE CORE FLOODED CLAD WORTH AT EOEC

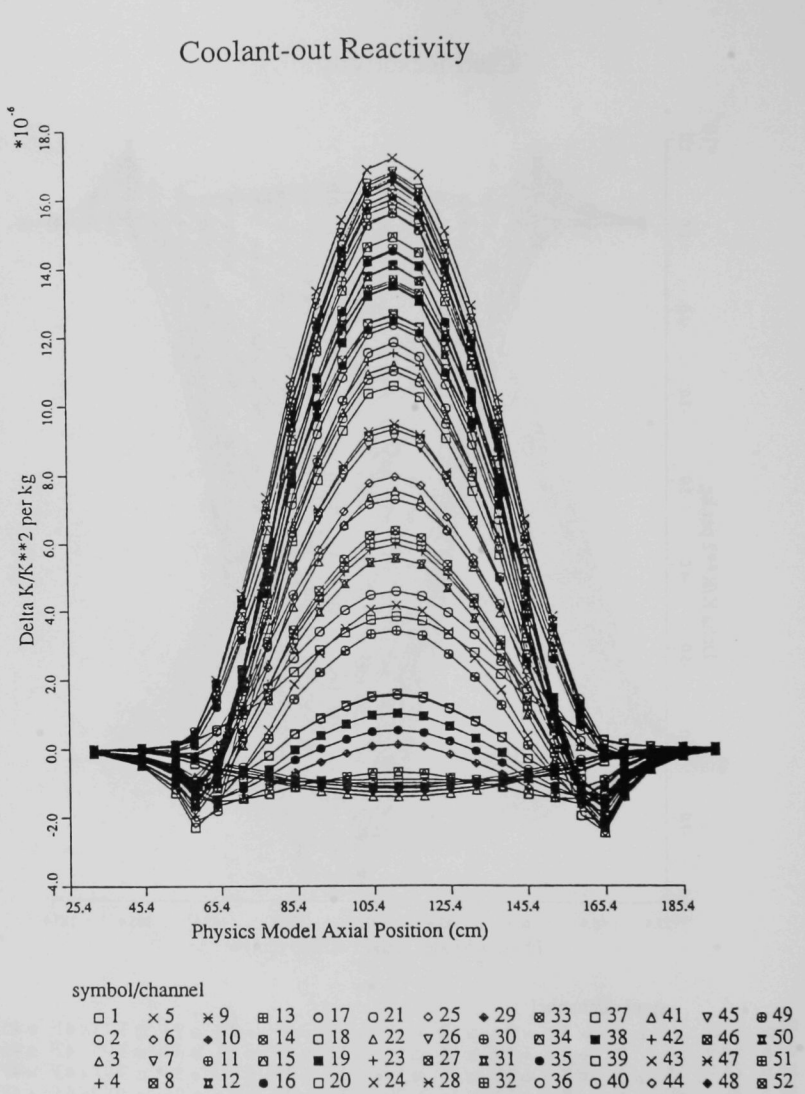

FIGURE 21. OXIDE CORE SODIUM DENSITY WORTH AT EOEC

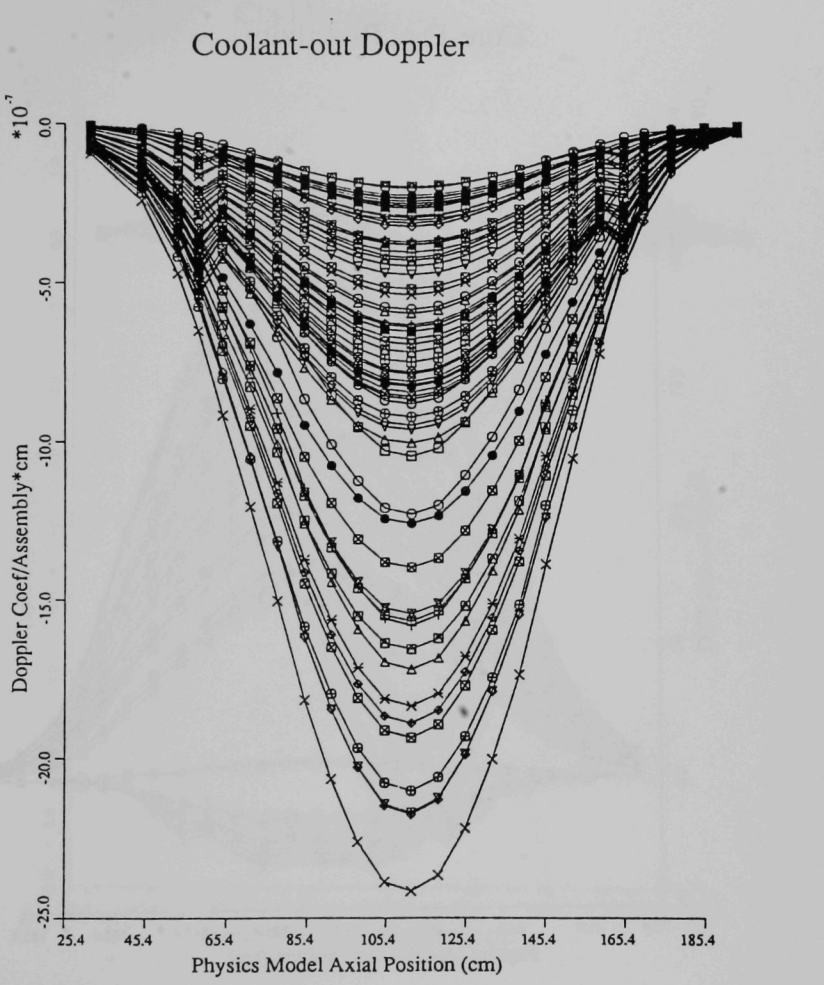

FIGURE 22. OXIDE CORE VOIDED DOPPLER WORTH AT EOEC

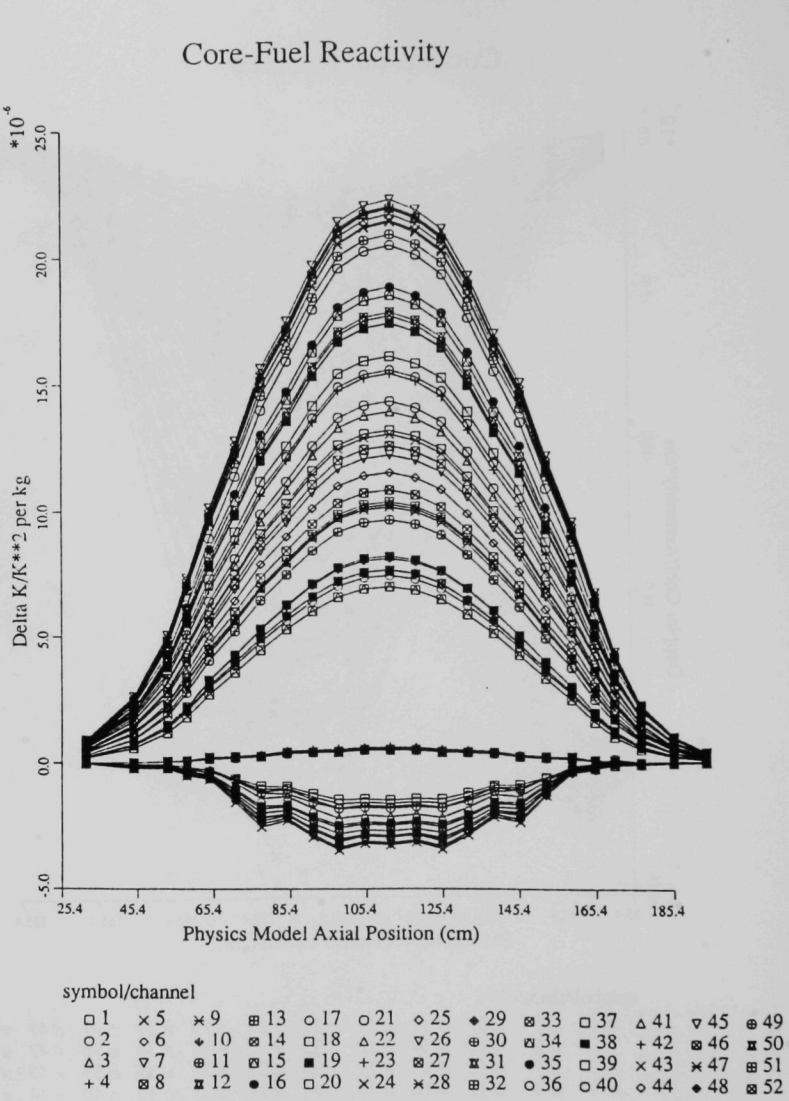

FIGURE 23. OXIDE CORE VOIDED FUEL WORTH AT EOEC

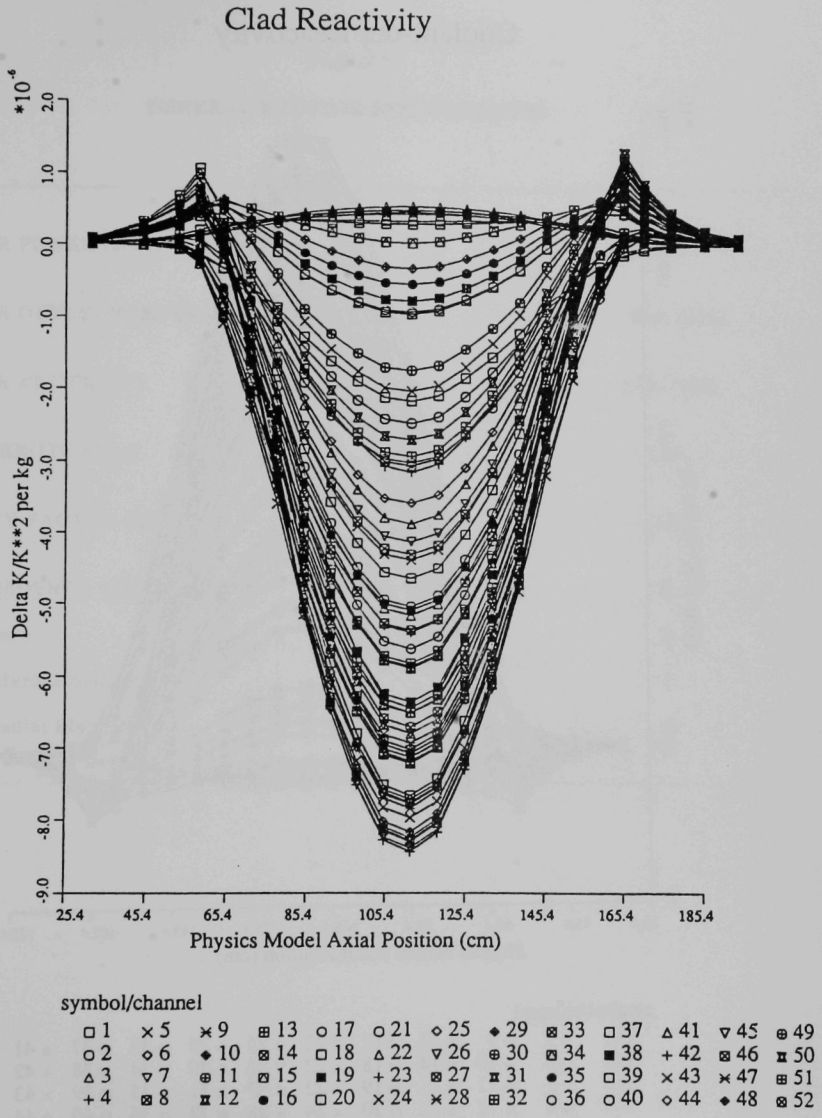

FIGURE 24. OXIDE CORE VOIDED CLAD WORTH AT EOEC

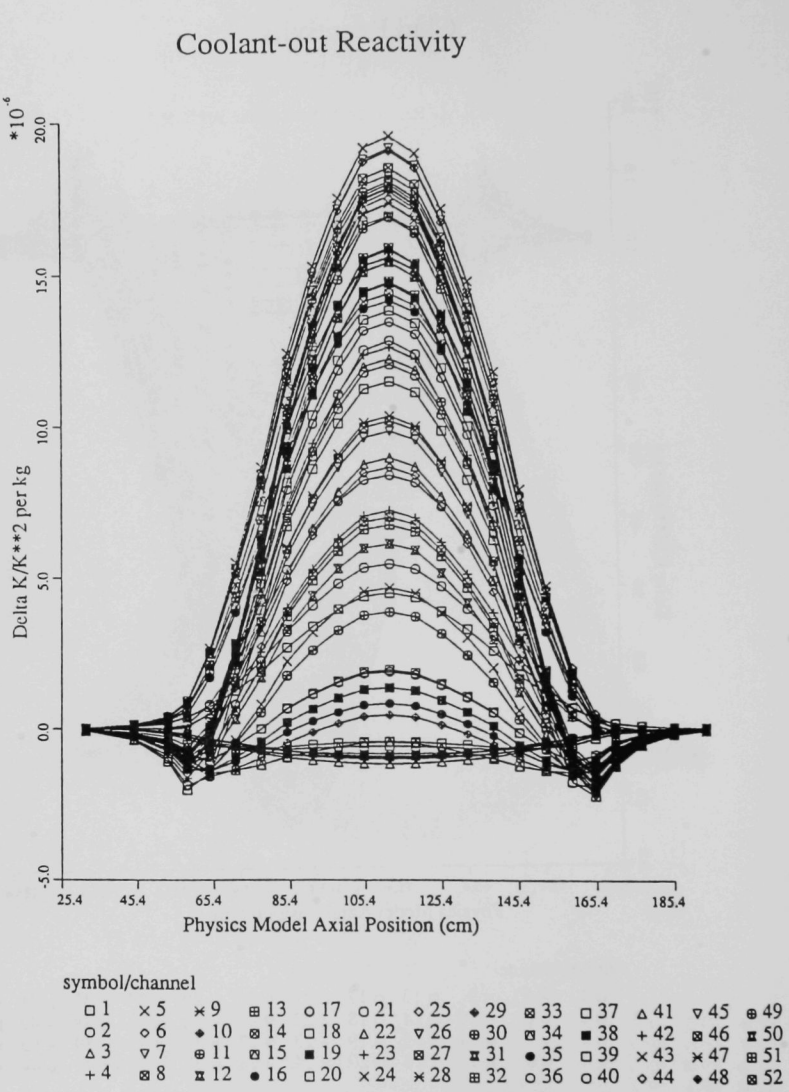

FIGURE 25. OXIDE CORE SODIUM VOID WORTH AT EOEC

TABLE I

GENERAL REACTOR SPECIFICATIONS

REACTOR POWER (MWt)	3500
REACTOR OUTLET TEMPERATURE (°F), (°C)	950, (510)
REACTOR ΔT (°F), (°C)	275, (153)
CYCLE LENGTH (days)	365
CAPACITY FACTOR (%)	80
FUEL RESIDENCE TIME (cycles)	
Core	3
Internal Blanket	3
Radial Blanket	6

TABLE II

GENERAL DESIGN CONSTRAINTS

	METAL	OXIDE
STRUCTURAL MATERIAL	HT-9	HT-9
DRIVER FLUENCE LIMIT (10^{22} fast nvt)	35	35
FUEL MATERIAL	UPu10Zr	UO_2PuO_2
DRIVER SMEAR DENSITY LIMIT	75 V/O	82.5 TD
PELLET DENSITY	15.7 gm/cc	86.8 TD
BURNUP LIMIT (MWd/kg HM)	150	150
BLANKET MATERIAL (depleted)	U10Zr	UO_2
PELLET DENSITY	15.7 gm/cc	95.7 TD
BLANKET SMEAR DENSITY LIMIT	85 V/O	93.3 TD
PEAK LINEAR HEAT RATING $(\frac{kW}{ft})$, $(\frac{w}{m})$	15 (317.5)	13.5 (285.8)

TABLE III

ASSEMBLY AND PIN DESIGN

	OXIDE	METAL
ASSEMBLY DESIGN		
Duct Design	hexagonal, nonvented	
Duct Pitch (in.)	6.131	6.131
Duct Wall Thickness (in.)	0.150	0.150
Duct Outer Flat-to-Flat (in.)	5.931	5.931
Inter-assembly Gap (in.)	0.200	0.200
Spacer Type	straight-start wire wrap (12 in. pitch)	
Number of Pins/Assembly (driver)	271	271
Number on Pins/Assembly (blanket)	169	169
P/D Ratio (driver)	1.18	1.18
P/D Ratio (blanket)	1.087	1.087
DRIVER FUEL PIN DESIGN		
Pin Outer Diameter (in.)	0.285	0.285
Cladding Thickness	0.022	0.022
Wire Spacer Diameter (in.)	0.049	0.049
Bond Type	He	Na
Pellet Density (% T.D.)	86.8	15.7 gm/cc
Smear Density (% T.D.)	82.5	75
Stoichiometry (O/M)	1.96	--
Fuel Length (in.)	40	36
Upper Axial Blanket Length (in.)	14	0
Lower Axial Blanket Length (in.)	14	0
Fission Gas Plenum Length (in.)	56	52
FUEL ASSEMBLY VOLUME FRACTIONS		
Fuel (smeared)	0.380	
Structure	0.260	
Sodium	0.360	

TABLE III

ASSEMBLY AND PIN DESIGN (Cont'd.)

	OXIDE	METAL
INTERNAL/RADIAL BLANKET PIN DESIGN		
Pin Outer Diameter (in.)	0.392	0.392
Cladding Thickness (in.)	0.022	0.022
Wire Spacer Diameter (in.)	0.034	0.034
Bond Type	He	Na
Pellet Density (% T.D.)	95.7	15.7 gm/cc
Smear Density (% T.D.)	93.3	85
Stoichiometry (O/M)	2.00	--
Blanket Length (in.)	68	36
Fission Gas Plenum Length (in.)	56	52
INTERNAL/RADIAL BLANKET ASSEMBLY		
Fuel (smeared)	0.495	
Structure	0.230	
Sodium	0.275	
CONTROL ASSEMBLY DESIGNS		
Control Material	Nat'l B_4C	
PRIMARY		
Control-In Volume Fractions		
B_4C (smeared)	0.390	
Structure	0.213	
Sodium	0.398	
Control-Out Volume Fractions		
Structure	0.067	
Sodium	0.933	

TABLE III

ASSEMBLY AND PIN DESIGN (Cont'd.)

	OXIDE	METAL
SECONDARY		
Control-In Volume Fractions		
B_4C (smeared)	0.301	
Structure	0.191	
Sodium	0.508	
Control-Out Volume Fractions		
Structure	0.125	
Sodium	0.875	
RADIAL STEEL SHIELD ASSEMBLY VOLUME FRACTIONS		
Shield Material	HT-9	
Structure	0.816	
Sodium	0.184	
RADIAL B_4C SHIELD ASSEMBLY VOLUME FRACTIONS		
Shield Material	Nat'l B_4C	
B_4C (smeared)	0.597	
Structure	0.219	
Sodium	0.184	

TABLE IV

NUMBER OF ASSEMBLIES

	OXIDE	METAL
DRIVERS	396	402
INTERNAL BLANKETS	163	157
RADIAL BLANKETS		
(1 row)	90	90
RADIAL SHIELDS		
Steel (1 row)	96	96
B_4C (2 rows)	210	210
CONTROL RODS		
Primary	24	24
Secondary	12	12

TABLE V

CONTROL SYSTEM ASSIGNMENT

	PRIMARY SYSTEM	SECONDARY SYSTEM
ROW 6	-	6 rods
ROW 9	6 rods	-
ROW 10	6 rods	-
ROW 13	12 rods	6 rods
TOTAL	24 rods	12 rods

TABLE VI

PLUTONIUM ISOTOPIC COMPOSITIONS (w/o)

	METAL		OXIDE		
	Equilibrium Loading	Equilibrium Discharge	Equilibrium Loading	Equilibrium Discharge	LWR Discharge
Pu 238	0.4	0.2	0.4	0.2	1.0
239	72.3	72.8	72.3	72.0	67.3
240	23.3	23.0	23.3	23.6	19.2
241	2.7	2.8	2.7	3.1	10.1
242	1.2	1.2	1.2	1.2	2.4

TABLE VII

METAL CORE EQUILIBRIUM MASS FLOW DATA

REACTOR POWER, MWE/MWTH : 1361/3500
FUEL RESIDENCE TIME, FPD : 3 X 252
CAPACITY FACTOR, % : 80

BOC KEFF - EOC KEFF :-6.177E-03
COMPOUND SYSTEM DOUBLING TIME, YRS : 41.2

	BREEDING RATIO	POWER SPLIT	SPEC.POWER KWTH/KGHM	BURNUP MWD/KG
CORE	0.595	81.942	93.700	82.081
INT.BLANKET	0.424	14.892	28.003	24.530
AX.BLANKET	0.0	0.0	0.0	0.0
RD.BLANKET	0.106	3.166	10.783	12.891
REACTOR TOTAL	1.126	100.000		

	U-235	U-236	U-238	PU238	PU239	PU240	PU241	PU242	TOTAL FISSILE	TOTAL HM
INITIAL LOADING,KG										
CORE	48.9	0.0	24690.1	23.4	4245.8	1370.2	157.5	72.2	4452.1	30607.9
IN.BLANKET	37.2	0.0	12576.1	0.0	0.0	0.0	0.0	0.0	37.2	18613.3
AX.BLANKET	0.0	0.0	0.0	0.0	0.0	0.0	0.0	0.0	0.0	0.0
RD.BLANKET	20.6	0.0	10256.7	0.0	0.0	0.0	0.0	0.0	20.6	10277.3
TOTAL	106.6	0.0	53522.8	23.4	4245.8	1370.2	157.5	72.2	4509.9	59498.4
EQUILIBRIUM LOADING,KG/YR										
CORE	16.3	0.0	8230.0	7.8	1415.3	456.7	52.5	24.1	1484.0	10202.6
IN.BLANKET	12.4	0.0	6192.0	0.0	0.0	0.0	0.0	0.0	12.4	6204.4
AX.BLANKET	0.0	0.0	0.0	0.0	0.0	0.0	0.0	0.0	0.0	0.0
RD.BLANKET	3.4	0.0	1709.5	0.0	0.0	0.0	0.0	0.0	3.4	1712.9
TOTAL	32.1	0.0	16131.5	7.8	1415.3	456.7	52.5	24.1	1499.9	18119.9
EQUILIBRIUM DISCHARGE,KG/YR										
CORE	8.8	1.4	7600.7	4.8	1164.9	468.4	58.2	25.3	1231.9	9332.6
IN.BLANKET	6.6	1.1	5719.6	0.0	304.3	17.0	0.6	0.0	311.6	6049.4
AX.BLANKET	0.0	0.0	0.0	0.0	0.0	0.0	0.0	0.0	0.0	0.0
RD.BLANKET	1.9	0.3	1594.7	0.0	72.1	4.8	0.2	0.0	80.2	1680.0
TOTAL	17.4	2.8	14915.1	4.8	1547.3	490.2	59.1	25.3	1623.7	17061.9
NET GAIN,KG/YR										
CORE	-7.4	1.4	-629.3	-3.0	-250.4	11.7	5.7	1.2	-252.1	-870.1
IN.BLANKET	-5.8	1.1	-472.4	0.0	304.3	17.0	0.6	0.0	299.2	-155.0
AX.BLANKET	0.0	0.0	0.0	0.0	0.0	0.0	0.0	0.0	0.0	0.0
RD.BLANKET	-1.5	0.3	-114.8	0.0	72.1	4.8	0.2	0.0	76.7	-32.9
TOTAL	-14.8	2.8	-1216.4	-3.0	132.0	33.5	6.6	1.3	123.8	-1058.0

NOTE : 1. FISSILE = PA233 + U233 + U235 + PU239 + PU241
2. BR AND CSDT CALCULATED WITH EQUAL FISSILE ISOTOPE WEIGHTING AND CREDIT FOR PA-233
3. CSDT CALCULATED WITH 1-YEAR EXTERNAL CYCLE TIME AND 1% REPROCESSING/FABRICATION LOSSES
4. EQUILIBRIUM LOADING AND DISCHARGE DATA ARE GIVEN IN TERMS OF EQUIVALENT ANNUAL MASS FLOW

TABLE VIII

OXIDE CORE EQUILIBRIUM MASS FLOW DATA

			BREEDING RATIO	POWER SPLIT	SPEC.POWER KWTH/KGHM	BURNUP MWD/KG
REACTOR POWER, MWE/MWTH	: 1361/3500	CORE	0.510	80.580	107.396	94.079
FUEL RESIDENCE TIME, FPD	: 3 X 252	INT.BLANKET	0.446	13.978	19.250	16.863
CAPACITY FACTOR, %	: 80	AX.BLANKET	0.157	2.489	4.354	3.814
		RD.BLANKET	0.109	2.953	7.095	12.430
BOC KEFF - EOC KEFF	: 5.255E-03					
COMPOUND SYSTEM DOUBLING TIME, YRS	: 23.2	REACTOR TOTAL	1.221	100.000		

	U-235	U-236	U-238	PU238	PU239	PU240	PU241	PU242	TOTAL FISSILE	TOTAL HM
INITIAL LOADING,KG										
CORE	38.7	0.0	19580.4	26.4	4804.5	1550.6	178.2	81.7	5021.5	26260.6
IN.BLANKET	50.8	0.0	25364.6	0.0	0.0	0.0	0.0	0.0	50.8	25415.4
AX.BLANKET	40.0	0.0	19965.0	0.0	0.0	0.0	0.0	0.0	40.0	20005.0
RD.BLANKET	29.1	0.0	14540.2	0.0	0.0	0.0	0.0	0.0	29.1	14569.4
TOTAL	158.7	0.0	79450.2	26.4	4804.5	1550.6	178.2	81.7	5141.5	86250.3
EQUILIBRIUM LOADING,KG/YR										
CORE	12.9	0.0	6526.8	8.8	1601.5	516.9	59.4	27.2	1673.8	8753.5
IN.BLANKET	16.9	0.0	8454.9	0.0	0.0	0.0	0.0	0.0	16.9	8471.8
AX.BLANKET	13.3	0.0	6655.0	0.0	0.0	0.0	0.0	0.0	13.3	6668.3
RD.BLANKET	4.9	0.0	2423.4	0.0	0.0	0.0	0.0	0.0	4.9	2428.2
TOTAL	48.1	0.0	24060.0	8.8	1601.5	516.9	59.4	27.2	1709.0	26321.9
EQUILIBRIUM DISCHARGE,KG/YR										
CORE	6.9	1.3	5976.7	5.5	1239.9	562.4	76.0	30.2	1322.8	7892.9
IN.BLANKET	10.5	1.4	7924.5	0.0	361.9	27.5	1.4	0.1	373.8	8327.3
AX.BLANKET	10.5	0.7	6475.9	0.0	149.0	6.5	0.3	0.0	159.7	6643.0
RD.BLANKET	3.1	0.4	2296.3	0.0	90.1	7.2	0.5	0.0	93.8	2397.7
TOTAL	31.0	3.9	22673.5	5.5	1841.0	603.7	78.2	30.3	1950.1	25266.9
NET GAIN,KG/YR										
CORE	-6.0	1.3	-550.1	-3.3	-361.6	45.6	16.6	3.0	-351.0	-859.6
IN.BLANKET	-6.5	1.4	-530.4	0.0	361.9	27.5	1.4	0.1	356.8	-144.5
AX.BLANKET	-2.9	0.7	-179.0	0.0	149.0	6.5	0.3	0.0	146.4	-25.6
RD.BLANKET	-1.7	0.4	-127.1	0.0	90.1	7.2	0.5	0.0	88.9	-30.5
TOTAL	-17.1	3.9	-1386.6	-3.3	239.5	86.8	18.8	3.1	241.1	-1055.0

NOTE : 1. FISSILE = PA233 + U233 + U235 + PU239 + PU241
2. BR AND CSDT CALCULATED WITH EQUAL FISSILE ISOTOPE WEIGHTING AND CREDIT FOR PA-233
3. CSDT CALCULATED WITH 1-YEAR EXTERNAL CYCLE TIME AND 1% REPROCESSING/FABRICATION LOSSES
4. EQUILIBRIUM LOADING AND DISCHARGE DATA ARE GIVEN IN TERMS OF EQUIVALENT ANNUAL MASS FLOW

TABLE IX

REACTOR MASS FLOW SUMMARY

		METAL	OXIDE
ENRICHMENT[a]	(%)	14.4	19.0
INITIAL FISSILE[a] LOADING	(kg fissile)	4,403.3	4,982.7
INITIAL HM LOADING	(tonne)	59.50	86.25
HEAVY METAL MASS FLOW RATE	(tonne/y)	18.12	26.32
BREEDING RATIO			
Drivers		0.595	0.510
Internal Blankets[b]		0.424	0.446
Radial Blankets[b]		0.106	0.109
Axial Blankets		-	0.157
TOTAL		1.126	1.221
NET FISSILE[a] PRODUCTION	(kg/y)	138.6	258.3

[a] $Pu^{239} + Pu^{241}$.

[b] Over full height; notice difference in heights of metal and driver IB's and RB's.

TABLE X

METAL CORE NEUTRON BALANCE

NEUTRON BALANCE

	REACTOR		CORE		AXIAL BLANKET		RADIAL BLANKET		INTERNAL BLANKET		CONTROL RODS	
	BOC	EOC	BOC	EOC	BOC	EOC	BOC	EOC	BOC	EOC	BOC	EOC
ETA OF FISSILE ISOTOPES	2.471	2.472	2.209	2.024	0.0	0.0	0.059	0.069	0.203	0.379	0.0	0.0
FERTILE FISSION BONUS	0.441	0.435	0.318	0.303	0.0	0.0	0.022	0.020	0.101	0.112	0.0	0.0
EXCESS NEUTRONS	1.912	1.907	1.638	1.512	0.0	0.0	0.055	0.059	0.219	0.336	0.0	0.0
NEUTRON LOSSES												
STRUCTURE	0.0	0.0	0.0	0.0	0.0	0.0	0.0	0.0	0.0	0.0	0.0	0.0
FISSION PRODUCTS	0.038	0.075	0.033	0.063	0.0	0.0	0.001	0.002	0.005	0.011	0.0	0.0
COOLANT	0.0	0.0	0.0	0.0	0.0	0.0	0.0	0.0	0.0	0.0	0.0	0.0
OTHER	0.129	0.128	0.085	0.083	0.0	0.0	0.009	0.008	0.035	0.037	0.0	0.0
SPECIAL ISOTOPES	0.0	0.0	0.0	0.0	0.0	0.0	0.0	0.0	0.0	0.0	0.0	0.0
TOTAL ABSORPTION LOSS	0.168	0.203	0.117	0.145	0.0	0.0	0.011	0.010	0.040	0.047	0.0	0.0
REACTIVITY CONTROL LOSS	-0.003	0.017	-0.002	0.013	0.0	0.0	-0.000	0.001	-0.000	0.003	0.0	0.0
LEAKAGE LOSS	0.591	0.573	0.906	0.766	0.0	0.0	-0.070	-0.050	-0.246	-0.143	0.0	0.0
TOTAL LOSSES	0.756	0.792	1.021	0.925	0.0	0.0	-0.059	-0.040	-0.207	-0.093	0.0	0.0
NET NEUTRONS FOR BREEDING	1.156	1.115	0.616	0.587	0.0	0.0	0.114	0.099	0.426	0.428	0.0	0.0

BOC FISSILE ABSORPTIONS = 1.621836E+19

EOC FISSILE ABSORPTIONS = 1.626117E+19

TABLE XI

OXIDE CORE NEUTRON BALANCE

NEUTRON BALANCE

	REACTOR		CORE		AXIAL BLANKET		RADIAL BLANKET		INTERNAL BLANKET		CONTROL RODS	
	BOC	EOC	BOC	EOC	BOC	EOC	BOC	EOC	BOC	EOC	BOC	EOC
ETA OF FISSILE ISOTOPES	2.294	2.286	2.030	1.834	0.031	0.057	0.052	0.061	0.181	0.334	0.0	0.0
FERTILE FISSION BONUS	0.352	0.353	0.243	0.235	0.014	0.016	0.016	0.015	0.078	0.087	0.0	0.0
EXCESS NEUTRONS	1.645	1.638	1.398	1.278	0.029	0.044	0.043	0.047	0.175	0.269	0.0	0.0
NEUTRON LOSSES												
STRUCTURE	0.0	0.0	0.0	0.0	0.0	0.0	0.0	0.0	0.0	0.0	0.0	0.0
FISSION PRODUCTS	0.045	0.087	0.038	0.073	0.000	0.001	0.001	0.002	0.005	0.012	0.0	0.0
COOLANT	0.0	0.0	0.0	0.0	0.0	0.0	0.0	0.0	0.0	0.0	0.0	0.0
OTHER	0.146	0.145	0.081	0.079	0.019	0.019	0.010	0.008	0.037	0.039	0.0	0.0
SPECIAL ISOTOPES	0.0	0.0	0.0	0.0	0.0	0.0	0.0	0.0	0.0	0.0	0.0	0.0
TOTAL ABSORPTION LOSS	0.191	0.233	0.118	0.151	0.019	0.020	0.011	0.010	0.043	0.051	0.0	0.0
REACTIVITY CONTROL LOSS	0.015	-0.000	0.012	-0.000	0.000	-0.000	0.000	-0.000	0.002	-0.000	0.0	0.0
LEAKAGE LOSS	0.191	0.188	0.741	0.622	-0.148	-0.135	-0.085	-0.066	-0.317	-0.232	0.0	0.0
TOTAL LOSSES	0.396	0.421	0.871	0.773	-0.128	-0.115	-0.074	-0.056	-0.273	-0.181	0.0	0.0
NET NEUTRONS FOR BREEDING	1.249	1.218	0.527	0.506	0.157	0.159	0.117	0.103	0.448	0.450	0.0	0.0

BOC FISSILE ABSORPTIONS = 1.796386E+19

EOC FISSILE ABSORPTIONS = 1.799003E+19

TABLE XII

POWER SPLIT (%)

	METAL		OXIDE	
	BOEC	EOEC	BOEC	EOEC
DRIVERS	83.4	77.3	82.4	75.6
INTERNAL BLANKETS	12.4	18.3	11.8	17.5
RADIAL BLANKETS	3.2	3.4	3.0	3.2
AXIAL BLANKETS	0	0	2.4	3.4

TABLE XIII

CORE LAYOUT OPTIMIZATION

	METAL CORE Fig. 1 Layout		OXIDE CORE Fig. 2 Layout		METAL CORE Fig. 2 Layout	
PEAKING FACTOR	1.42	1.49	1.44	1.52	1.51	1.63
PEAK ASSEMBLY POWER DENSITY (kw/ℓ)						
Inner Core	456	486	471	467	570	570
Middle Core	533	530	480	468	570	552
Outer Core	546	503	486	443	519	496
BURNUP CONTROL SWING (% Δk)	+0.62 optimized for Metal		-0.53 optimized for Oxide		+0.91 non-optimal	

TABLE XIV

PEAK LINEAR HEAT RATINGS

	METAL		OXIDE	
	BOEC	EOEC	BOEC	EOEC
AS CALCULATED				
Driver	12.88	12.51	11.47	11.05
Internal Blankets	8.69	12.76	6.91	10.57
Radial Blankets	6.31	6.19	4.98	4.92
WITH CORRECTION FOR FRESH ASSEMBLIES				
Driver	13.85	13.35	12.50	11.97
Internal Blankets	12.34	15.55	10.17	12.97
Radial Blankets	9.12	8.21	7.31	6.58

TABLE XV

DISCHARGE BURNUPS

	METAL		OXIDE	
	Average	Peak	Average	Peak
DRIVERS	79.7	114.3	90.9	133.7
INTERNAL BLANKETS	23.8	39.7	16.3	42.3
RADIAL BLANKETS	18.3	45.7	12.0	47.7
AXIAL BLANKETS	-	-	3.7	15.4

TABLE XVI
PEAK DISCHARGE FLUENCE

	METAL	OXIDE
PEAK DISCHARGE FLUENCE		
(fast nvt * 10^{22})		
Driver	31	23
Internal Blankets	30	21
Radial Blankets	38	28

TABLE XVII
ESTIMATE OF METAL CONTROL SYSTEM REQUIREMENTS (%Δk)

	PRIMARY SYSTEM	SECONDARY SYSTEM
HOT-TO-COLD[a]	0.387±0.077	0.228±0.046
REACTIVITY FAULT[b]/ SHUTDOWN MARGIN[c]	0.039/0.352	0.039/0.352
REACTIVITY EXCESS[d]	0.618±0.293	-
CRITICALITY UNCERTAINTY[e]	±0.3	-
FISSILE TOLERANCE[f]	±0.3	-
TOTAL REQUIREMENT	1.357±0.521	0.580±0.046
MAXIMUM REQUIREMENT	1.878	0.626

[a]Determined from total reactivity increase associated with decrease in temperature from operating temperature to refueling temperature (505°K) for primary system or to standby temperature (630°K) for secondary system. A 20% uncertainty is assumed.

[b]Based on runout of one row-9 primary rod from maximum insertion (9.14 cm) at EOEC and a rod interaction factor of 1.5.

[c]A shutdown margin of 1.0$ is used because it exceeds the rod-runout worth.

[d]An uncertainty of 15% of the nominal value +0.2%Δk is assumed.

[e]Assumed equal to CRBR value.

[f]Based on an uncertainty of 0.5% in batch fissile enrichments.

TABLE XVIII

ESTIMATE OF OXIDE CONTROL SYSTEM REQUIREMENTS (%Δk)

	PRIMARY SYSTEM	SECONDARY SYSTEM
HOT-TO-COLD[a]	1.059±0.212	0.763±0.153
REACTIVITY FAULT[b]/ SHUTDOWN MARGIN[c]	0.033/0.330	0.033/0.330
REACTIVITY EXCESS[d]	0.526±0.279	-
CRITICALITY UNCERTAINTY[e]	±0.3	-
FISSILE TOLERANCE[f]	±0.3	-
TOTAL REQUIREMENT	1.915±0.550	1.093±0.153
MAXIMUM REQUIREMENT	2.465	1.246

[a]Determined from total reactivity increase associated with decrease in temperature from operating temperature to refueling temperature (505°K) for primary system or to standby temperature (630°K) for secondary system. A 20% uncertainty is assumed.

[b]Based on runout of one row-9 primary rod from maximum insertion (10.2 cm) at BOEC and a rod interaction factor of 1.5.

[c]A shutdown margin of 1.0$ is used because it exceeds the rod-runout worth.

[d]An uncertainty of 15% of the nominal value +0.2%Δk is assumed.

[e]Assumed equal to CRBR value.

[f]Based on an uncertainty of 0.5% in batch fissile enrichments.

TABLE XIX

METAL CORE CONTROL BANK WORTHS

	PRIMARY	SECONDARY
TOTAL WORTH	4.17% Δk	1.80% Δk
STUCK ROD	0.34% Δk[a]	0.20% Δk[b]
MINIMUM WORTH	3.83% Δk	1.60% Δk

[a]Based on a stuck row 9 primary rod.

[b]Based on a stuck row 6 secondary rod.

TABLE XX

OXIDE CORE CONTROL BANK WORTHS

	PRIMARY	SECONDARY
TOTAL WORTH	4.43% Δk	1.99% Δk
STUCK ROD	0.28% Δk[a]	0.26% Δk[b]
MINIMUM WORTH	4.15% Δk	1.73% Δk

[a]Based on a stuck row 9 primary rod.

[b]Based on a stuck row 6 secondary rod.

TABLE 21

EFFECTIVE DELAYED NEUTRON PARAMETERS

	METAL CORE			OXIDE CORE		
EFFECTIVE DELAYED FRACTION, β	0.003515			0.003301		
PROMPT GENERATION, (sec.)	$3.19 \cdot 10^{-7}$			$4.07 \cdot 10^{-7}$		
FAM	BETA(I)	A(I)	LAMBDA(I)	BETA(I)	A(I)	LAMBDA(I)
1	7.8193D-05	2.2244D-02	1.2992D-02	7.7617D-05	2.3510D-02	1.2975D-02
2	7.2703D-04	2.0682D-01	3.1411D-02	7.0629D-04	2.1393D-01	3.1326D-02
3	6.4233D-04	1.8272D-01	1.3559D-01	6.1353D-04	1.8583D-01	1.3507D-01
4	1.2756D-03	3.6288D-01	3.4752D-01	1.1900D-03	3.6043D-01	3.4613D-01
5	6.0094D-04	1.7095D-01	1.3807D+00	5.4445D-04	1.6491D-01	1.3792D+00
6	1.9117D-04	5.4383D-02	3.7919D+00	1.6962D-04	5.1378D-02	3.7497D+00

TABLE XXII

REACTIVITY FEEDBACK COEFFICIENTS AT EOEC

	METAL		OXIDE	
BETA EFFECTIVE	$3.515 \cdot 10^{-3}$		$3.301 \cdot 10^{-3}$	
PROMPT NEUTRON LIFETIME, (s)	$3.195 \cdot 10^{-7}$		$4.054 \cdot 10^{-7}$	
SODIUM VOID WORTH, ($)				
Driver	4.98		3.79	
IB	2.31		1.68	
RB	-0.03		-0.08	
AB	-		-0.19	
SODIUM DENSITY WORTH, ($)				
Driver	4.51		3.37	
IB	1.99		1.42	
RB	-0.06		-0.11	
AB	-		-0.23	
DOPPLER COEFFICIENT, $\left(-10^{-3} T \frac{dk}{dT}\right)$	Fuel	Structure[a]	Fuel	Structure[a]
Flooded Doppler				
Driver	1.929	0.508	3.984	0.968
IB	1.726	0.174	4.337	0.380
RB	0.181	0.015	0.406	0.030
AB	-	-	0.592	0.065
Voided Doppler				
Driver	1.155	0.378	2.933	0.710
IB	1.180	0.136	3.518	0.293
RB	0.138	0.012	0.340	0.023
AB	-	-	0.506	0.052

TABLE XXII

REACTIVITY FEEDBACK COEFFICIENTS AT EOEC (cont'd)

	METAL	OXIDE
AXIAL EXPANSION COEFFICIENT, ($/cm)		
Fuel		
Driver	-0.718	-0.693
IB	0.081	0.137
RB	-0.004	-0.007
Fuel and Clad		
Driver	-0.641	-0.617
IB	0.118	0.170
RB	-0.007	-0.009
Fuel and Total Structure		
Driver	-0.586	-0.562
IB	0.145	0.195
RB	-0.008	-0.010
RADIAL EXPANSION COEFFICIENT, ($/cm)	-0.765	-0.640
CONTROL ROD DRIVELINE EXPANSION COEFFICIENT[b,c], ($/cm)	-0.116	-0.0712

[a] Structure Doppler includes clad plus duct wall.

[b] Value at BOEC = -0.0785 $/cm metal; -0.1183 $/cm oxide.

[c] See Table XXIII for bank positions at BOEC and EOEC.

TABLE XXIII

CONTROL ROD BANK LOCATIONS[a]
(used to determine control rod driveline expansion coefficient)

	PRIMARY BANK		SECONDARY BANK	
	BOEC	EOEC	BOEC	EOEC
METAL	0	3.6	0	0
OXIDE	4.0	0	0	0

[a]Expressed as inches of insertion relative to the top of the driver fuel.

TABLE XXIV

AXIAL MESH INTERVALS USED IN COMPUTING SAS-CHANNEL WORTH DISTRIBUTIONS IN THE METAL CORE

AXIAL REGION	MODELED LENGTH[a] (in.)	NUMBER OF MESH INTERVALS	MESH WIDTH (in.)
UPPER PLENUM	4	2	2
CORE	36	20	1.8
LOWER SHIELD	4	2	2

[a]The pointwise reactivity distribution was tabulated for the axial segment labeled "modeled length". However, the neutronic solution was performed over a much larger axial height.

TABLE XXV

AXIAL MESH INTERVALS USED IN COMPUTING SAS-CHANNEL WORTH DISTRIBUTIONS IN THE OXIDE CORE

AXIAL REGION	MODELED LENGTH[a] (in.)	NUMBER OF MESH INTERVALS	MESH WIDTH (in.)
UPPER AXIAL BLANKET SEGMENT	10	2	5
UPPER AXIAL BLANKET SEGMENT	4	2	2
CORE	40	15	2.667
LOWER AXIAL BLANKET SEGMENT	4	2	2
LOWER AXIAL BLANKET SEGMENT	10	2	5

[a]The pointwise reactivity distribution was tabulated for the axial segment labeled "modeled length". However, the neutronic solution was performed over a much larger axial height.

VI. REFERENCES

1. D. C. Wade and Y. I. Chang, "The Integral Fast Reactor (IFR) Concept: Physics of Operation and Safety," Proc. Int'l Topical Meeting on Advances in Reactor Physics, Mathematics, and Computation, Paris, Vol. 1, pp. 311-336 (April 1987).

2. E. B. Baumeister and R. T. Lancet, "SAFR Plant Fuel Cycle Studies," Trans. Am. Nucl. Soc., 49, 88 (1985).

3. E. A. Aitken, I. N. Taylor, and M. L. Thompson, "Fuel Cycle for the Power Reactor Inherently Safe Module," Trans, Am. Nucl. Soc., 49, 87 (1985).

4. L. C. Walters, B. R. Seidel, and J. H. Kittel, "Performance of Metallic Fuels and Blankets in Liquid-Metal Fast Breeder Reactors," Nucl. Technol., 65, 179 (1984).

5. H. P. Planchon, J. I. Sackett, G. H. Golden, and R. H. Sevy, "Implication of the EBR-II Inherent Safety Demonstration Test," Nuclear Engineering and Design, 101, pp. 75-90 (1987).

6. H. Henryson II, B. J. Toppel, and C. G. Stenberg, "MC^2-2: A Code to Calculate Fast Neutron Spectra and Multigroup Cross Sections," ANL-8144, Argonne National Laboratory (1976).

7. W. M. Stacey, Jr., et al., "A New Space-Dependent Fast-Neutron Multigroup Cross-Section Preparation Capability," Trans. Am. Nucl. Soc., 15, 292 (1972).

8. B. J. Toppel, "A User's Guide to the REBUS-3 Fuel Cycle Analysis Capability," ANL-83-2, Argonne National Laboratory (1983).

9. R. D. Lawrence, "The DIF3D Nodal Neutronics Option for Two- and Three-Dimensional Diffusion Theory Calculations in Hexagonal Geometry," ANL-83-1, Argonne National Laboratory (1983).

10. K. L. Derstine, "DIF3D: A Code to Solve One- Two-, and Three-Dimensional Finite-Difference Diffusion Theory Problems," ANL-82-64, Argonne National Laboratory (1984).

11. F. E. Dunn, et al., "The SASSYS-1 LMFBR Systems Analysis Code," Proc. International Meeting on Fast Reactor Safety, Knoxville, TN, CONF-850410, Vol. 2, p. 999 (April 1985).

12. R. A. Wigeland, R. B. Turski, and R. L. Lo, personal communication, Argonne National Laboratory (March 1989).

B